Treatment of TCE-DNAPL Source Zones using Nanoscale Iron:
Treatability Studies with Z-Loy™

A thesis

submitted by

Katherine Merriam

In partial fulfillment of the requirements
for the degree of

Master of Science
in
Civil and Environmental Engineering

TUFTS UNIVERSITY
August 2011

Advisor: C. Andrew Ramsburg

Abstract

Treatability studies were conducted to explore the extent to which Z-Loy, a commercially-available suspension of nanoscale, reactive iron particles, can transform TCE-DNAPL within a heterogeneous source zone. The surface-normalized, pseudo-first-order rate coefficient for TCE degradation with Z-Loy was determined to be $(8.77 \pm 0.15) \times 10^{-4}$ L/m^2-hr ($(8.77 \pm 0.15) \times 10^{-4}$ L/g-hr) in batch experiments. Primary degradation products in these experiments were found to be ethene and ethane. The rate of TCE degradation using Z-Loy is comparable to other iron products being marketed as nanoscale ZVI. Two dimensional aquifer cell studies were conducted to examine the combined transport and reaction within a heterogeneous DNAPL source zone. Results from these experiments suggest Z-Loy has limited transport in the subsurface. Average mass discharges downstream of the Z-Loy were decreased by 85% over the course of a 14 day treatment period. Reductions in mass discharge were attributed to the combined effect of reaction and flow field alteration (Z-Loy reduced the flow through the treated zone). Effluent samples collected from the aquifer cell suggest 2.03 mmol TCE (of 160 mmol initially present) were reacted. Overall results suggest that the use of Z-Loy may hold promise for containment, but should not be viewed as a source reduction technology.

Acknowledgements.

Special thanks to Dr. C. Andrew Ramsburg for his guidance on this Master's Thesis. Additional thanks to my Thesis Committee, Dr. Kurt Pennell and Dr. Grant Garven for their input. Finally, thank you to Dr. Nicole Berge, Ms. Rhiannon Ervin, and Mr. Douglas Walker for their assistance in the IMPES Laboratory. On Materials, LLC is gratefully acknowledged for their donation of the Z-Loy used herein. This research was sponsored by Strategic Environmental Research and Development Program Project ER-1487 (contract W912HQ-06-C-0032) and National Science Foundation Award CMMI 1000714.

Table of Contents

1. Introduction. 7
2. Literature Review. 9
    2.1 Nanoscale Iron Particle Kinetics. 9
    2.2. Types of nanoscale iron 12
    2.3. Summary of Dechlorination Rate Data. 16
    2.4. Preliminary Z-Loy Reactivity Study. 18
        2.4.1.Effect of Groundwater Characteristics on Reactivity. 18
        2.4.2. Effect of DO and ORP on Particle Reactivity. 19
        2.4.3.Effect of Particle Age, pH, and Hydrogen Production on Particle Reactivity. 19
        2.4.4. Effect of Common Groundwater Ions on Reaction Kinetics. 21
        2.4.5. Effect of TCE concentration on Kinetic Reactivity and Reaction within the NAPL. 23
    2.5. Transport of Enhanced Iron Particles in Porous Media. 25
    2.6. Comparison of Transport: Bare Nanoparticles and Stabilized Particles. 30
    2.7. Emulsified Iron Transport through Porous Media. 30
    2.8. Comparison of Transport Abilities of Bare Nanoparticles to Surface Enhanced Particles. 33
    2.9. Iron Treatments within the Context of Partial Source Zone Removal. 34
        2.9.1. Implications of Partial Source Zone Treatment 36
3. Objectives. 38
4. Batch Experiment Materials and Methods. 40
    4.1.Chemicals. 40
    4.2.Z-Loy Suspension Preparation. 40
    4.3.Batch Reactors. 41
    4.4.Analytical. 41
    4.5. Iron Characterization. 43
    4.6.Reaction Rates. 43
    4.7. MATLAB Program. 45
    4.8.Aquifer Cell Studies. 45
5.Results and Discussion. 49
    5.1.Batch Reactivity. 49
    5.2. Aquifer Cell Experiments. 58
        5.2.1. Experiment A – Z-Loy Transport though a TCE-DNAPL source. 59
        5.2.2. Experiment B - Injection within a DNAPL-Source 67
6. Conclusions 80

List of Tables.

Table 1. Summary of Iron Nanoparticle Rate Data 17
Table 2. Iron Particle Enhancements 28
Table 3. Summary of kinetic batch experiments 50
Table 4. Aquifer Cell Properties 58

List of Figures.

Figure 1. Possible TCE Reduction Pathways 11
Figure 2. Aquifer Cell Schematic 46
Figure 3. Batch data and model fits for the reaction of TCE with Z-Loy: Z-Loy Shipment I in Milli-Q water 53
Figure 4. Batch data and model fits for the reaction of TCE with Z-Loy: Z-Loy shipment III in Milli-Q water 54
Figure 5. Batch data and model fits for the reaction of TCE with Z-Loy: Z-Loy in 0.11 M NaBr and 0.10 M NaCl. 55
Figure 6. Hydrogen Production in Batch Reactors 1-4 56
Figure 7. Side port sampling locations in Experiments A and B. 59
Figure 8. TCE Effluent Data (Aquifer Cell #1) 60
Figure 9. TCE Port Data (Aquifer Cell #1) 61
Figure 10. Aquifer Cell #1 Tracer Tests (Pre and Post Z-Loy Injection) 62
Figure 11. Aquifer Cell #1: During Final Z-Loy Injection 63
Figure 12. Aquifer Cell #1: 0.25 Pore Volumes After Final Z-Loy Injection 63
Figure 13. Aquifer Cell #1: 0.75 Pore Volumes After Final Z-Loy Injection 64
Figure 14. H_2 Production in Reactor Containing Z-Loy and 0.021 mM Erioglaucine A 65
Figure 15. H_2 Production in Reactors Before and After Addition of Erioglaucine 66
Figure 16. Effluent TCE Concentrations (Aquifer Cell #2) 68
Figure 17. Effluent Ethene and Ethane Concentration (Aquifer Cell #2) 68
Figure 18. Port 1 Concentrations (Aquifer Cell #2) 69
Figure 19. Port 2 Concentrations (Aquifer Cell #2) 69
Figure 20. Port 3 Concentrations (Aquifer Cell #2) 70
Figure 21. Port 4 Concentrations (Aquifer Cell #2) 70
Figure 22. Cl^- Effluent Concentration (Aquifer Cell #2) 73
Figure 23. Recovery and transformation of TCE in Aquifer Cell #2 (Negative Pore Volumes are Prior to Z-Loy Injecton) 74
Figure 24. Aquifer Cell #2 Tracer Tests (Pre and Post Z-Loy Injection) 76
Figure 25. Aquifer Cell #2: 0.2 Pore Volumes of Dyed Tracer Introduction 76
Figure 26. Aquifer Cell #2: 0.35 Pore Volumes of Dyed Tracer Introduction 77
Figure 27. Aquifer Cell #2: 0.5 Pore Volumes of Dyed Tracer Introduction 77
Figure 28. Aquifer Cell #2: 0.75 Pore Volumes of Dyed Tracer Introduction 77
Figure 29. Source Zone, Pre Z-Loy 78
Figure 30. Source Zone Saturation, Pre Z-Loy 78
Figure 31. Source Zone, Post Z-Loy 78
Figure 32. Source Zone Saturation, Post Z-Loy 78

1. Introduction.

Chlorinated solvents prominent in the subsurface in the form of DNAPLs (dense non-aqueous phase liquids) are a source of persistent halogenated organic contaminants (HOCs). If these sources can be removed or lessened, site cleanup time can be significantly reduced. In recent years, iron filings have been used in the form of permeable reactive barriers to reduce trichloroethylene (TCE) plumes. In this reaction, the iron is oxidized and supplies electrons and the TCE is reduced and releases chloride ions. The reaction pathways are beta elimination, hydrogenation and hydrogenolysis. Over recent years, interest in using nanoscale zero valent iron particles (nZVI) and bimetallic particles(Fe-Pd and Fe-Ni) has increased due to their high surface to volume ratio and catalyst addition which yields greater TCE dechlorination rates than iron filings.

Remediation efforts must not only be effective at reducing TCE source zone mass, they must be able to effectively transport through the subsurface to ensure that they encounter the source zone as well. Iron nanoparticle transport may be affected by diffusion, interception (particle/soil and particle/particle interactions), straining following aggregation, and sedimentation, which lead to pore clogging and particle aggregation. The possibility of flow bypass and source zone mobilization must be taken into account for treatability analyses and iron injection as well.

Surface enhanced nanoscale ZVI particles have been shown to have higher rates of dechlorination, as well as better transport capabilities than bare nanoparticles alone. Z-Loy, a commercial grade nanoscale iron particle provided by OnMaterials, was examined for means of DNAPL source zone remediation. Z-Loy is a desirable product due to its advertised high surface area, small particle size, hydrogenation catalyst, and limited aggregation. The reaction kinetics, daughter products produced, transport capabilities, and potential for source zone reduction with Z-Loy were examined and determined in this study.

2. Literature Review.

A literature review was conducted to gain proper understanding of advances made in iron nanoparticle research for use of TCE reduction and delivery to NAPL source zones. Specific focused was placed on hydrogen reduced, borhydride reduced, and bimetallic nanoparticle kinetics, which may perform similarly to the iron in this study. Z-Loy is an aqueous iron nanoparticle suspension; therefore, emphasis was also placed on comparing the transport capabilities of surface enhanced iron nanoparticles relative to those that were unenhanced. Finally, a study of partial source zone removal and its implications for this study were examined.

2.1 Nanoscale Iron Particle Kinetics.

In the past, treatment of chlorinated solvents using iron particles focused on permeable reactive barriers (PRBs). However, more recently, iron nanoparticles have been examined due to their high specific surface area and potentially high transport capabilities. Studies have shown that both iron filings (used in PRBs) and iron nanoparticles (for direct injection into the subsurface) have similar surface normalized TCE degradation rates (10^{-3} $Lh^{-1}m^{-2}$ for nanoscale iron and approximately 10^{-4}-10^{-3} $Lhr^{-1}m^{-2}$ for iron filings)(Johnson et al., 1996; Tratnyek and Johnson, 2006).

This is a summative order of magnitude comparison of iron filings and iron nanoparticles (temporarily excluding bimetallic particles). The mass of nanoscale iron needed for TCE reduction is determined by the Fe^0 content available in the particles, as well as the selectiveness of the reaction for TCE reduction. The half reactions of interest are (Hering and Schnoor, 2000):

$$Fe^0 \rightarrow Fe^{2+} + 2e^- \quad (1)$$

$$TCE + ne^- + mH^+ \rightarrow products + 3Cl^- \quad (2)$$

$$2H^+ + 2e^- \rightarrow H_2\uparrow \quad (3)$$

$$\text{Full Balanced Equation: } Fe^0 + TCE \rightarrow Fe^{2+} + products + nCl^- \quad (4)$$

The available electrons in these half reactions are consumed to produce H_2 or reduce TCE. The amount of TCE dechlorinated per mass of Fe^0 delivered will depend on the above half-reactions (i.e.,the value of n which is a function of product distribution), the availability and accessibility of Fe^0 in the core, and the extent of H_2 production. The iron may also interact with water or the dissolved oxygen, which results in the following passive corrosison reactions (Hering and Schnoor, 2000).

$$2Fe^0(s) + O_2(g) + 4H^+(aq) \rightarrow 2Fe^{2+}(aq) + 2H_2O(l) \quad (5)$$

$$Fe^0(s) + 2H^+(aq) \rightarrow Fe^{2+}(aq) + H_2(g) \quad (6)$$

The best description of the paths by which TCE can be reduced by Fe^0 was produced by Arnold and Roberts (2000). Their overview of the possible reactions is shown in Figure 1.

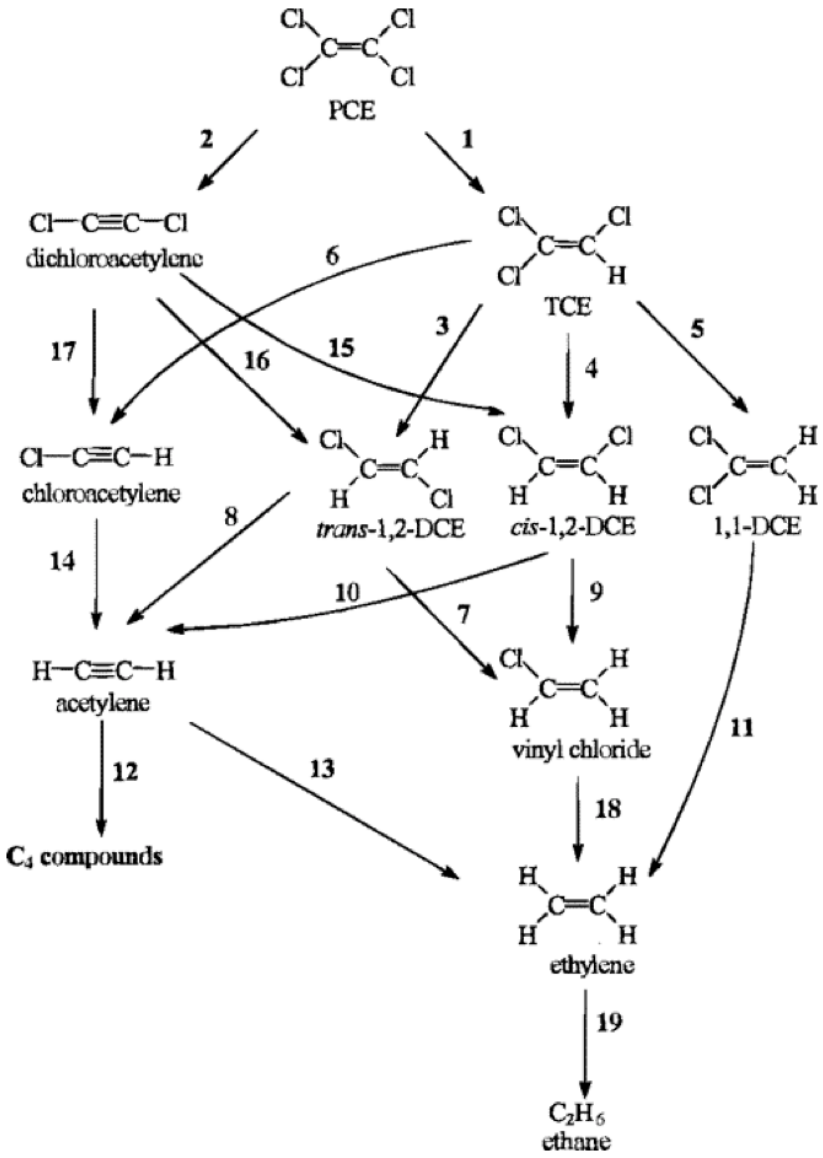

Figure 1. Possible TCE Reduction Pathways (Arnold and Roberts, 2000)

Reactions 1, 3, 4, 5, 7, 9, 14, 17, and 18 correspond to hydrogenolysis reactions (carbon/chloride bond is cleaved and the chloride is replaced with hydrogen),

while reactions 2, 6, 8, and 10 are reductive β-elimination reactions (carbon/chloride bonds are broken with chlorides released and additional bonds added between the carbon atoms), reaction 11 proceeds via reductive α-elimination (two carbon/chloride bonds are broken, with chloride released and replaced by hydrogen), and reactions 13, 15, 16, and 19 are hydrogenation reactions(carbon/carbon bonds are broken and replaced with carbon/hydrogen bonds). The direct conversion of TCE to ethene is believed to be the main reduction pathway in this study, which is completed through hydrogenolysis. It should be noted that there can be reaction branching off and therefore competing reactions for such pathways. The pathways taken often may depend on the type of iron utilized in the study.

Over the recent years, advancements in iron nanoparticles have been made. Two of the most prominent advancements have been the creation of nanoscale bimetallic particles and surface modified nanoscale iron particles. Both of which have been extensively studied and are discussed in the following sections.

2.2. Types of nanoscale iron

Four of the types of iron nanoparticles that are studied today are hydrogen reduced iron particles (RNIP), borohydride reduced particles (Fe/B), plasma vapor deposition produced particles, and bimetallic particles (produced typically

with Palladium (Pd) and Platinum (Pt)). Focus here (section 2.2) will be placed on RNIP, Fe/B, and bimetallic particles.

Liu and Lowry (2005) studied iron particles synthesized by aqueous phase reduction of ferrous or ferric iron using sodium borohydride (Fe/B). Additionally, they examined reactive nanoscale iron particles (RNIP) that were synthesized by gas-phase reduction of iron oxides in H_2 (commercially available from Toda Kogyo Corporation, Onoda, Japan). Under iron limiting conditions(initial TCE concentration of 290 mg/L), Fe/B reduced TCE to 87.4% even-numbered saturated alkanes. The produced ethene was transformed to ethane, with no detectable acetylene. cDCE and vinyl chloride were found to be intermediates, but were transformed quickly. RNIP (initial TCE concentration of 290 mg/L) transformed TCE to mostly acetylene (84.3%) and ethene (7.8%) under iron limiting conditions with minute amounts of cis-DCE and vinyl chloride present at the end of the reaction (exhaustion of the reactive iron). Fe/B demonstrated zero order kinetics (due to Langmuir-Hinshelwood-Hougen-Watson kinetics and iron reactive sites filled with TCE) assuming direct pathways to radical coupling products, ethene, and ethane. RNIP yielded pseudo-first order reaction kinetics assuming direct pathways to acetylene and ethane. Fe/B also yields more saturated daughter products, showing a higher rate of hydrogenation compared to iron filings that could be explained by the catalytic reaction pathway. It is also noted that there is no deactivation during dechlorination suggesting that the iron oxide/iron hydroxide shell is continuously reactive or that particles are dissolving

during reaction to ensure reactive sites are available(which also explains the determined 92% electron efficiency of Fe/B for dechlorination). In contrast, RNIP's kinetics and low TCE/Fe ratio lead to the hypothesis that TCE is weakly adsorbed to the particle surface, there are excess reactive sites, or another factor is controlling the reaction. The rates found for RNIP are similar to iron filings and dechlorination is explained by assuming beta elimination and a direct pathway to ethane. RNIP also displayed evidence of first order deactivation (0.29/day) when conditions were iron-limiting, which is most likely caused by a growing Fe_3O_4 shell during the reaction which hinders electron transfer from the core to the exterior. RNIP's electron efficiency is much lower than Fe/B due to the excess H_2 present, as well as the inaccessibility of some Fe^0.

Zhang et al. (2003) examined Pt/Fe and Pd/Fe bimetallic particles, with Pt and Pd acting as catalysts, while Fe acts as the electron donor, which would effectively reduce chlorinated solvents (TCA and TCE). These iron particles were coated with a thin layer of metal catalyst by saturating the wet iron precipitates with an ethanol solution, causing reduction and deposition of the metal on the iron surface (Zhang, 1998). In batch experiments containing 6.25 g/L Pd/Fe (initial TCE concentration of 4.68 mg/L), all chlorinated compounds were at concentrations below detection limits of 10 ug/L within 8 hours, with ethane as the dominant daughter product. These particles can achieve a dechlorination rate of about 1 mg TCE/ g nano Fe/h and have a total capacity of about 100-200 mg TCE/ g nano Fe (both of which are 1-3 orders of magnitude higher than iron powders).

Furthermore, Lin et al. (2004) assessed the ability of Pd or Pt to increase reaction rates between iron nanoparticles. A spontaneous redox reaction occurs as the metals are deposited onto the iron's surface. The oxidized states of these metals were Pd^0, Pt^0, Pt(II), and Pt(IV). The magnitude of dechlorination rate increase compared to untreated iron for Pd and Pt bimetallic particles were 23.3 ± 4.8 and 0.041 ± 0.009, respectively. The distribution of chlorinated products were similar for both particle types (*cis*-DCE at 51%; 1,1-DCE at 27%; *trans*-DCE at 15% and VC at 7%). Additionally, an increase in hydrogen production was observed for both types of particles, leading to a faster dechlorination rate (initial reaction was cathodically controlled).

Elliot and Zhang (2001) propose a core/shell model with an iron oxide shell and embedded catalyst of Pd or Ni, with a Fe^0 core. Electrons from Fe^0 core oxidation are transported through the shell and reduce adsorbed TCE. Batch experiments (initial TCE concentration of 4.45 to 8 mg/L) found complete dechlorination of TCE after 12 h in reactors with 0.25 g Fe/Pd and 2 days in reactors containing 0.1 g Fe/Pd, compared to one month in reactors containing unsynthesized iron particles. Again, ethene and ethane were the dominant daughter products. Finally, Shrick et al. (2002) focused on the reductive capabilities of Ni/Fe bimetallic particles. These particle yielded 50-80 times faster dechlorinaion rates than bare iron nanoparticles and iron filings. However, the long term presence of Ni in the subsurface may be of environmental concern.

2.3. Summary of Dechlorination Rate Data.

The kinetics of many types of iron particles were summarized in Berge and Ramsburg (2010). This summary is reproduced here as Table 1 with the addition of some recent studies.

Table 1. Summary of Iron Nanoparticle Rate Data

Iron	Reported (L/h m2)	Initial Concentration (mM)	Initial Concentration (mg/L)	Reference
Hydrogen Reduced Iron Particles (HR)	0.001	0.027	3.55	Liu et al. (2007)
HR	0.0012	0.11	14.45	Liu et al. (2007)
HR	0.0012	0.46	60.44	Liu et al. (2007)
HR	0.0004	2.21	290	Liu et al. (2005a)
HR	0.00078	8.4	1,103	Liu et al. (2007)
Borohydride Reduced Iron Particles (BH)	0.002	0.03	3.94	Liu et al. (2005a)
BH	0.0027	0.08	10.51	Wang et al. (2010)
BH	0.089	0.08	10.51	Song and Carraway(2008)
BH-Pd (0.42 wt.% Pd)	0.14	0.13	17.08	Meyer et al. (2009)
BH-Pd (0.42 wt.% Pd)	0.019	0.15	19.71	Meyer et al. (2009)
BH-Pd (5 wt.% Pd)	0.012	0.91	120	Lien and Zhang (2007)
BH-Pd (20 wt.% Pd)	0.037	0.08	10.51	Tee et al. (2005)
BH-Pd (Pd is 0.1% w/w Fe) particles coated with CMC	1.56	0.38	49.93	He et al. (2007)
Carbon particles with physisorbed CMC containing Fe-Pd: 0.8 wt.% CMC, 1 g/L Fe particles, 0.05% (w/w iron particles)	0.0447	0.152	19.97	Zhan et al. (2009)
HR coated with various polyelectrolytes	0.00073-0.00014	8.4	1,103	Phenrat et al. (2009)
BH coated with poly(methyl methacrylate)	0.00077	0.08	10.51	Wang et al. (2010)
CMC-stabilized FePd bimetallic nanoparticles	2.427	0.1145	15.05	Cho and Choi (2010)
Starched palladized iron (Fe−Pd) nanoparticles	0.020	0.1908	25.07	He and Zhao (2005)
Gum Arabic Oil-in-water Emulsion	0.0015	N/A	N/A	Long and Ramsburg (2010)

2.4. Preliminary Z-Loy Reactivity Study.

Phenrat et al. (2010) were the first to report on the kinetics of the Z-Loy iron nanoparticles with TCE. Z-Loy is a sub-micrometer zero valent iron suspension with tailorable surface areas (1-30 m^2/g) and the optional addition of hydrogenation catalysts (e.g. Pd, Cu). Z-Loy's reaction rate constant was determined to be $301 \pm 14 \times 10^{-3}$ L/g-hr($10 \pm 4.66 \times 10^{-3}$ L/m^2-hr). The daughter products produced were mainly ethane, with a small amount of ethene. Based on the high reaction rate and large presence of ethane, a reduction through a catalytic pathway is a possibility. Approximately 5 mol% of the reaction products were chlorinated intermediates such as 1,1-DCE, t-DCE, and *cis*-DCE. It was noted that although Z-Loy had a high reaction rate, the lifetime of the reaction was short, and was exhausted after 3-4 days.

2.4.1.Effect of Groundwater Characteristics on Reactivity.

Once the kinetics of iron nanoparticles are determined, it is necessary to examine the effect that common groundwater conditions may have on enhancing or hindering reactivity. Many of these characteristics have been extensively studied and are described in detail below.

2.4.2. Effect of DO and ORP on Particle Reactivity.

High DO levels and positive ORP measurements demonstrate an oxidizing environment. Phenrat et al. (2009), hypothesized such conditions to be a disadvantage regarding zero valent iron applications because DO can utilize electrons from the iron by the formation of water and superoxide radicals, causing a competing reaction (iron oxidation due to dissolved oxygen can use electrons that would be otherwise available.) If Fe^{2+} is further oxidized to Fe^{3+} in an oxic environment, iron hydroxides can precipitate and coat the surface of the iron particle, leading to particle passivation and slower reaction rates.

2.4.3.Effect of Particle Age, pH, and Hydrogen Production on Particle Reactivity.

Liu and Lowry (2005) examined the effect of H_2 evolution on reactivity of Fe/B and RNIP. When H_2 was added to reactor headspace instead of argon, the time it took to eliminate TCE from the system reduced from 72 hours to 22 hr for Fe/B and the product distribution was very similar to those found with excess iron in the reactor. There was no change in TCE reaction rate for RNIP. In another study, the H_2 production of RNIP containing 9.6% Fe^0 content was observed over 50 days (Liu et al., 2006). With respect to Fe^0 content, the H_2 production was pseudo first order. Decreasing pH between 8.0 and 6.5 was observed to increase the rate of H_2 production (Liu and Lowry, 2006). Experiments conducted above pH 8.0 suggest the rate of H_2 production becomes relatively independent of pH

under basic conditions. With respect to TCE degradation rates using RNIP, decreasing the pH from 8.9 to 6.5 doubled the observed reaction rate coefficient (which was an order of magnitude less than that observed for H_2 production). This demonstrates a first order trend (albeit weak) for the influence of pH on the rate coefficient. This weak dependence of TCE dechlorination on H^+ and Fe^0 content leads to the conclusion that electron transfer is not the main factor controlling TCE reduction rates. Furthermore, it should be noted that Wang and Farrell (2003) found that reduction occurs primarily through atomic hydrogen at low pH values, which at neutral pH values, is primarily via direct electron transfer and atomic hydrogen. Electric induction(i.e., electron transfer reactions) values at higher pH levels were higher and the slow diffusion of absorbed atomic hydrogen to a cathodic site leading to electron transfer to TCE is a smaller rate limitation.

Liu et al. (2006) focused on the effect of particle age (Fe^0 content) on nZVI reactivity. The Fe^0 content of the nZVI particles and the pH of the solution can effect H_2 production and TCE dechlorination. Past studies have produced mixed results regarding the effect of particle age on reactivity. Column studies showed an exponential decay in TCE reduction over a span of three years (Klausen et al., 2003). This could be due to an increase in Fe-oxide and Fe-(oxy)-hydroxides formed on the particle surface which then reduces reactivity or because of decreases in porosity and therefore access to nZVI particles.

The Fe^0 content for the reactors studied by Liu et al. (2006) ranged from 48 ± 0.2% for fresh particles (19 days in slurry before being dried) to 9.6 ± 0.4% for highest oxidation (210 days in slurry before drying.) It was noted that the particle surface did not change greatly during oxidation in water and that the Fe^0 core shrinks while the magnetite shell grows at the interface of Fe^0 and Fe_3O_4. Consistent results showed that the H_2 production is proportional to the initial Fe^0 content of the particles, demonstrating a first order reaction of H_2 production regarding Fe^0 content. TCE reactivity decreased in all observations as the particles aged.

2.4.4. Effect of Common Groundwater Ions on Reaction Kinetics.

Common groundwater constituents such as Cl^-, NO_3^-, HCO_3^-, SO_4^{2-}, and HPO_4^{2-} can affect the reactivity of nZVI by the following mechanisms. NO_3 (an Fe^0 reducing solute) presence may lead to competition of reactive cathodic sites (Farrell, 2000). Additionally, HCO_3^-, SO_4^{2-}, HPO_4^{2-} may limit access to reactive sites due by creation of an oxide layer (Devlin and Allin, 2005). However, presence of Cl^-, HCO_3^-, and SO_4^{2-} may yield increased reactivity by dissolution of the iron oxide layer (Devlin and Allin, 2005). Liu et al. (2007), added RNIP (with 48% Fe_0 content) to batch reactors containing 5 mN of individual solutes (Cl^-, NO_3^-, HCO_3^-, SO_4^{2-}, HPO_4^{2-}). Due to the competition that NO_3^- has for reactive sites, special emphasis was placed on this solute. It was found that for NO_3^- concentrations less than 1 mN, there was a slight increase in TCE reaction rates.

This lack of reaction decrease implies that at low concentrations, there is little NO_3^- surface coverage on the RNIP due to the low affinity that NO_3^- has for the negative RNIP surface. For NO_3^- concentrations greater than 3 mN, TCE reduction decreased with increased NO_3^- solution concentration. This reduction in reactivity may be due to competition between NO_3^- and TCE to reactive sites or due to nZVI surface passivation, which alters the reduction reaction from cathodic to anodic control (reduction of TCE to release of electrons and Fe^{2+}). It was also noted that H_2 production was mostly unaffected by NO_3 concentrations.

The other groundwater solutes considered do not compete for electrons or atomic H, yet reactivity was decreased in the following order for every solute present, Cl^- $<SO_4^{2-}<HCO_3^-<$ HPO_4^{2-} (at pH=8.9). This order is consistent with the affinity of anion complexation to hydrous ferric oxide considering known stability constants (Moore and Young, 2005). This infers that the reduction in TCE transformation is caused by Fe-anion complexes formed on the nZVI surface, leading to passivation of reactive sites. The fact that HCO_3^- and HPO_4^{2-} both have a larger effect on TCE reduction could be due to the formation of precipitation of Fe-carbonate and Fe-phosphate on the RNIP surface. Finally, although this study focused on RNIP, it should be mentioned that poisoning of catalysts (due to ions such as Cl^-) may lead to decreased reactivity in bimetallic particles (Sivasanker, 2002).

2.4.5. Effect of TCE concentration on Kinetic Reactivity and Reaction within the NAPL.

Liu et al. (2007) studied the effect of TCE concentration on batch reactivity. In the case of RNIP, TCE reduction decreased with increased TCE concentration. This effect was attributed to iron passivation and reactive site saturation. For TCE concentrations ranging from 0.027 to 0.46 mM, pseudo first order dechlorination kinetics were observed. A decrease of reactivity by two times was observed from the lowest to highest TCE concentrations and increased TCE concentration inhibited the particle lifetimes. The increase in TCE concentration also led to greater production of acetylene as the daughter product. Liu et al. (2007) suggested that this was probably due to TCE competing with acetylene for reactive sites, as well as less atomic H being adsorbed to the ZVI surface, which leads to less reduced reaction products.

Because TCE concentration strongly influences particle reactivity, it is important to examine iron particle reactivity with TCE concentrations near solubility, as well as within the DNAPL phase to determine if ZVI particles are a viable treatment option for NAPL source zones. Quinn et al. (2005) examined the ability of encapsulated iron to treat a field scale test area with dissolved TCE concentrations up to solubility. For all depths of TCE concentrations, significant reductions were observed (57-100%). Additionally, the average reduction in downgradient concentration was 68% and the mass flux reduction was 56%.

Reactions occurring within the NAPL phase or at the NAPL-water interface may not be limited by contaminant dissolution or transport (Berge and Ramsburg, 2010). Berge and Ramsburg (2010) determined that iron particles in the NAPL phase have dechlorination rates proportional to the concentration of soluble water in the NAPL. For their experiments, RNIP was reacted with TCE with varying water contents. The reaction rates observed were lower than aqueous phase rates, but the reaction did not slow over a 12 day observation period. Additionally, the higher the water content of the NAPL, the higher the utilization of the available electrons is, and that reactions within the NAPL may be as efficient (in terms of electrons going toward degradation) as reactions within the aqueous phase. Taghavy et al. (2010) studied the effects of iron particles injected into a PCE-DNAPL column with 5.5% residual saturation. The end result was 30% conversion to ethene, 50% removed in the dissolved phase, and 20% remaining in DNAPL form. There was no noticeable reduction in PCE effluent sampling, remaining near equilibrium solubility concentrations (yet reaction occurred based on significant ethene production. Minimal H_2 production was observed, consistent with Liu and Lowry's (2006) findings, which state that hydrogen evolution decreases with increased chlorinated solvent concentrations. Saleh et al. (2007) developed the concept of targeting the source zone using hydrophobic coatings, which help to transfer the iron particles through the porous medium and target the NAPL-water interface. Amphiphilic triblock copolymers with high hydrophobe/hydrophile ratios have a lower elution rate in columns packed with dodecane coated sand than clean sand alone, signifying an affinity for the

dodecane-water interface. However, it should be noted that batch studies conducted with these particles and NAPL phase TCE yielded lower reactivites by magnitudes of 2 to 10.

2.5. Transport of Enhanced Iron Particles in Porous Media.

Iron particle transport in porous media may be hindered by particle/soil and particle/particle interactions (Phenrat et al., 2007; Tratnyek and Johnson, 2006). According to filtration theory, the transport of colloidal particles through porous media is controlled by interception, Brownian diffusion, and sedimentation. Filtration theory assumes that colloids are being filtered through a homogenous wet-packed media. When accounting for attachment (interception) of colloids through the subsurface and ignoring detachment, the first order attachment rate coefficient (k) can be found in the following equation (Flury and Qui, 2007).

$$k = \frac{3}{2}\frac{(1-\theta)}{d}\alpha\eta\nu \qquad (8)$$

Where, θ is the effective porosity of the media, d is the effective particle size of the media, α is the collision efficiency factor, η is the single collector efficiency, and ν is the pore water velocity. Additionally, deep bed filtration theory ignores particle agglomeration (particle concentration) and the effect of previously attached particles on deposition, and assumes that attachment efficiency is controlled solely by nanoparticle-collector interactions (Phenrat et.al., 2009). Consistent with theory, nanoparticle slurries at low particle concentrations have attachment coefficients solely controlled by nanoparticle-collector interactions.

Therefore, reactive iron slurries and suspensions containing dispersants, liquid membranes, surface coatings, and iron coating on carrier particles are being examined for delivery enhancement of source zone treatment applications. Advances have also been made to create more stable dispersants utilizing surfactants, starch, polymers, modified cellulose, and vegetable oil (Zhan et al., 2008).

Numerous surface enhancement techniques have been employed to improve the stability, reactivity, and transport of iron nanoparticles. One of the main downfalls of creating iron particles within an aqueous solution is particle agglomeration, which is mostly due to particle-particle interactions via the long-range magnetic force (Cushing et al., 2004). Particle surface enhancements have been studied over previous years to improve these suspension. Mallouk et al. (2004) used carbon nanoparticles and poly(acrylic acid) (PAA) to stabilize iron nanoparticles. Furthermore, Sun and Zhang (2005) concluded that polyvinyl alcohols could reduce the size of the particles and aggregates.

He et al. (2007) claimed that water-based suspensions of iron particles are most advantageous due to minimal use of harmful chemicals/solvents. According to He et al. (2007), cellulose can be modified to sodium carboxymethyl cellulose (CMC). CMC is low cost, not harmful to the environment, water-soluble, and has been successfully used to stabilize superparamagnetic iron oxide nanoparticles (SPIONs) and Ag nanoparticles. They concluded that stabilization of iron

nanoparticles could be achieved due to the CMC molecules onto the surface of the nanoparticles. The CMC acts as a protective layer that hinders the nanoparticle growth and prevents agglomeration through the electrostatic repulsion and steric hindrance. The reactivity of the enhanced particles was then compared with unenhanced. When 0.2% CMC was used, k_{obs} increased from 0.44 to 7.4 h^{-1}. Almost all TCE was destroyed within 40 minutes. During reduction, VC and *cis*- or *trans*-DCE were not detected and trace amounts of 1,1-DCE were detected initially, but were not detectable at the end of monitoring. The chloride production rate was nearly stoichiometrically coupled the TCE degradation rate.

Further summary of the various types of iron particle enhancements is shown in Table 2 below.

Table 2. Iron Particle Enhancements

Iron Product	Porous Medium	Flow Control Method	Flow Direction	Published Breakthrough Curved	Darcy Velocity (m/d)	Particle Mass in Suspension (g/L)	Particle Retention
Iron prepared with borohydride reduction/coated with Tween 20 (Kanel et al. 2007)	Glass Beads and sand (30% water saturation)	Constant Flow	Downward	Yes	9	1	72% in glass beads/61% in sand/65% in baked sand
Iron prepared based on borohydride reduction and coated with 0.3 – 1.2% polyacrylic acid (Kanel and Choi 2007)	Glass Beads	Constant Flow	Upward	Yes	2-15	5	N/A
Iron prepared based on borohydride reduction and supported by hydrophilic carbon and polyacrylic acid (Schrick et al. 2004	Ottawa Sand and Hagerstown, Pope, and Chagrin soils	Constant Head	Downward	Yes	13-127	5	Strong retention for unenhanced iron/ 40-100% for polyacrylic acic supported iron/ 99-0% for hydrophilic carbon supported iron
Iron prepared based on borohydride reduction with 0.8% wt. sodium carboxymethyl cellulose addition and subsequent coating with palladium (He et al. 2007	Loamy Sand	Variable Head	Downward	No	Not reported	1	99.8% for unsupported iron/ 2% for iron palladium particles coated with sodium carboxymethyl celulose

Iron prepared based on borohydride reduction and coated with 1% vol. polyacrylic acid (Yang et al. 2007	Silica Sand	Variable Head	Downward	No	34	2.5	Complete retention for unmodified/ Effective transport for polyacrylic acid coated
Reactive nanoscale Iron Product (Toda America, Inc.) coated with amphiphilic polymers (2 g/L) (Saleh et al. 2007	Silica sand	Constant Flow	Horizontal	No	31	3	98.6% for bare particles/ 5% for PSS-650 modified particles
Reactive Nanoscale Iron Product (Toda America, Inc.) coated with gum agar (0.5 g/L) (Tiraferri and Sethi, 2009)	Silica Sand	Constant Flow	Downward	Yes	7.9 and 40	0.154	N/A
Laboratory synthesized iron combined with ethylsilica (manufactured: aerosol-assisted technique) (Zhan et al., 2008	Ottawa Sand	Constant Flow	Downward	Yes	515	3	30%
Oil-in-water Emulsion (Berge and Ramsburg, 2009)	Silica sand	Constant Flow	Upward	Yes	0.4	2.5	0.17-0.3%
CMC Stabilized Particles (He et al. 2009)	Glass Beads Sand Sandy Soil	Constant Flow	Upward	Yes	0.03	0.2	N/A
poly(styrene sulfonate) (PSS) modified NZVI (Phenrat et al., 2009)	Silica Sand	Constant Flow	Upward	Yes	0.32	5	N/A
Aqueous RNIP suspension with 3.5 mM of calcium chloride (Taghavy et al., 2010)	Silica Sand	Constant Flow	Downward	Yes	14.7	60	N/A

2.6. Comparison of Transport: Bare Nanoparticles and Stabilized Particles.

Zhan et al. (2008) compared the transport capabilities of bare nanoscale iron particles to surface enhanced particles. Specifically, they compared uncoated RNIP to ZVI entrapped in porous silica particles (prepared using an aerosol assisted process). After running 10 mL of bulk suspension of both particles types through a 10 cm column packed with Ottawa sand, and flushing with 60 mL, it is clear that the enhanced particles had superior transport ability. RNIP was trapped within the first few centimeters, while the Fe/ethylsilica particles, flushed through the entire column. Almost 70% of the Fe/ethylsilica suspension was collected through its breakthrough curve, while no significant amount of RNIP was in the column effluent. The transport of these particles through capillaries was also observed through optical microscopy. Glass tubes were packed with Ottawa sand and were injected with the particle suspensions, followed by water flushing. RNIP again was trapped near the inlet, while the Fe/ethylsilica particles were more normally distributed throughout the entire tube. Finally, the Fe/ethylsilica particles were found to be able to partition into the water/TCE interface, which can lead to better access of bulk TCE.

2.7. Emulsified Iron Transport through Porous Media.

Berge and Ramsburg (2009) then attempted to expand upon the current delivery enhancements available using kinetically stable soybean oil-in-water emulsions

(which limit iron corrosion during injection) that transport through porous media with ease (less than 0.30 % iron retained in the column). Oleic acid, Aerosol MA, Aerosol OT, and Span 80 surface coatings were found to enhance the emulsion's stability. Long and Ramsburg (2010) also studied Gum Arabic stabilized oil in water emulsions as a mean for iron particle enhancement with a density of 1.15 g/mL. Gum Arabic(GA) is a non toxic, natural material produced from sap of Acacia senegal, Acacia seyal or Acacia polyacantha that is commonly used in the food industry(Dickenson, 2003). In this study, the ability of GA to stabilize soybean oil in water emulsions with high concentration of ZVI particles was determined. These emulsions were deemed kinetically stable for 4 hours, with destablization occurring by sedimentation over the next 4 days. Surface normalized rate coefficients found within the oil droplets were equivalent to aqueous phase rate coefficients of about 5×10^{-3} L/m^2h. These rates are comparable to rates found for aqueous iron particle suspensions.

Crocker et al. (2007) explored the stability of the combination of Z-Loy and oil-in-water emulsions. The emulsion composition was comprised of 10% wt. tallow oil, 2% wt. Span 80, 6% wt. Tween 80, and was 0.05% wt. iron (0.11% wt. metal) with a density of 0.9 g/mL. The emulsion stability was tested with and without iron. It should be noted that when iron was added to the emulsion, approximately three times the amount of surfactant was needed to keep the emulsion stable for greater than one hour. Effluent Z-Loy recovery for the Z-Loy/oil-in-water emulsion was 99% wt, due to the high amount of surfactant used. Although there

was head loss during emulsion flushing, it is not due to pore clogging, but is the result of fluid viscosity.

Examining DNAPL mobilization more closely, the total trapping number, N_T, was used to determine conditions to limit mobilization (Pennell et al. 1996). Results from N_T analyses conducted by Berge and Ramsburg (2009) and Long and Ramsburg (2011) suggest that the iron containing oil-in-water emulsions developed by these authors can be delivered at meaningful velocities (e.g., 1 m/d) within a medium sand without mobilizing entrapped DNAPL. This result is in contrast to other emulsion based approaches which have higher viscosity (e.g., ~2000 cP, Quinn et al. 2005). High viscosity emulsions must therefore be implemented using a slow velocity (e.g., 1 m/d in the same medium sand) to prevent DNAPL mobilization. Another concern regarding emulsion enhanced delivery is pore clogging (Soo and Radke, 1984). However, in their study, Berge and Ramsburg (2009) observed near complete recovery of the emulsion which exhibited breakthrough that was well aligned with the conservative, non-reactive tracer. This leads to the assumption that the emulsion has little/no effects on long term permeability (Soo and Radke, 1984).

2.8. Comparison of 2-dimensional Transport Abilities of Bare Nanoparticles to Surface Enhanced Particles.

Kanel and Choi (2007) were among the first to examine the two-dimensional transport capabilities of surface stabilized zero valent iron particles. As previously stated, iron nanoparticles have an inherent nature to aggregate due their magnetism (Kanel et al. 2007). Therefore, actions must be taken to stabilize the particles for implementation into porous media. The synthesized particles were synthesized/stabilized with poly acrylic acid (PAA) and were found to be stable up to 60 days (compared to 1-10 min for unstabilized particles). The synthesized particles, along with unenhanced particles and a non-reactive tracer, were injected into a two-dimensional flow container and compared. The tracer dispersed and was transported horizontally through the porous media in a matter of minutes. The surface enhanced zero valent iron particles moved horizontally and downward through the flowfield. This is due to the higher density of the particle suspension than water (1.036 g/cm^3 to 1 g/cm^3, respectively). Unlike both the tracer and the enhanced iron particles, the bare nanoparticles were unable to effectively transport through the flow field. This lack of transport is most likely due to hydrophobic/hydrophilic interactions, changes in attachment efficiency due to ionic strength and steric stabilizations, and the blocking of deposition sites (Lecoanet et al., 2004). It is also noted that the bare nanoparticle suspension has a positive charge at neutral pH, and the porous media was negatively charged, leading to charge interactions and iron particle attachment to

the porous medium. The enhanced iron particle transport showed only slight retardation with respect to the tracer and had enhanced transport relative to the bare particles because of the association of the hydrophobic component of the PAA with the iron particles and the positioning of the polar headgroup regarding the aqueous phase. The surface enhanced suspension also maintained a negative charge at neutral pH values, stabilized by the anionic polymer, preventing strong interactions with the porous media. Finally, it is believed that the surface enhanced suspension's transport is controlled by advection and dispersion processes coupled to small-scale density gradients.

2.9. Iron Treatments within the Context of Partial Source Zone Removal.

It should be noted that in the field, complete mass removal of the source mass is often not achieved. Therefore, it is important to examine partial source zone removal. Previous studies based on mathematical dissolution have shown varying results. Sale and McWhorter (2001) determined that almost total source zone mass removal is required to minimize mass flux to drinking water standards using analytical solutions for the dissolution of ganglia and pools in uniform flow fields. However, Wood et al. (2005) utilized a stream tube modeling approach to conclude that 60% reduction in source zone mass leads to 80% decrease in mass flux.

Suchomel and Pennell (2006) studied the effect that limited source zone removal of tetrachloroethylene (PCE) had on dissolved phase contaminant flux using a two-dimensional aquifer cell. Initial source zone saturation distributions were quantified by light transmission analysis and specified as ganglia to pool (GTP) ratios ranging from 0.16 to 1.6. Ganglia are formed when capillary forces keep discontinuous droplets within the cell's pores and these ganglia are not mobile under typical flow conditions. Pools may form when low permeability zones are present and the DNAPL accumulates across the less permeable layers surface. DNAPL distributions are affected by the volume and rate of DNAPL release, density, interfacial tension, viscosity, and the permeability and wettability of the porous medium and these distributions alter the effectiveness of remediation efforts. For the cell with GTP=1.6 (high GTP), about 75% of the mass was reduced after two Tween 80 floods (intermediated by a water flood). The rate and amount of PCE recovery was greater during the first surfactant flood due to dissolution of ganglia rather than low interfacial area pools. For the cell with a GTP=0.4 (mid GTP), three surfactant floods with two separating water floods were conducted, with a final mass removal of 92% and similar recovery efficiencies were observed for the mid/low GTP aquifer cell. Finally, for the low GTP cell (GTP=0.16), 57.4% of the total PCE mass was recovered during three surfactant floods and two water floods.

These findings support the fact that dissolution based remediation techniques are limited by the GTP (interfacial area that allows mass transfer to occur). In the

high GTP aquifer cell, mass discharge and effluent concentration remained constant after 50% PCE source removal (due to remaining ganglia in the system). After 85% of the source mass as ganglia was removed, the mass discharge was reduced by 60%. It is apparent that source zone mass removal may need to be large in ganglia dominated source zones to ensure greatly reduced mass discharge. In contrast, for pool dominated source zones, more minimal mass removal is necessary for reduced mass discharge (Rao et al., 1997).

2.9.1. Implications of Partial Source Zone Treatment

If it is assumed that the ZVI is fully converted to Fe^{2+}, the mass ratio of iron needed per mass of TCE is 0.42:1. Therefore, to achieve 50% mass removal, about 7.72 g of ZVI must be delivered in the case of this study. It is possible that one cannot deliver enough ZVI to such a source zone, and if it is delivered, reactivity may not be maintained. Use of iron to contain a source zone may become a concern, if dissolution overwhelms the rate and extent of reaction - that is, TCE is still discharged (Taghavy et al. 2010). Additionally, direct injection of ZVI into the source zone can lead to NAPL mobilization. Illangasekare et al. (2009), suggest implementing iron particles both within and immediately down gradient of the source zone to effectively treat the NAPL contamination. Additionally, Taghavy et al. (2010) determined that implementing ZVI particles to the dissolved phase downstream of the source zone increases both particle efficiency and reactivity.

Treatment within the DNAPL source zone remains an open question, particularly for particles/amendments which are designed and marketed to be well transported and bimetallic (e.g., Z-Loy) and a faster reaction may keep up with source zone dissolution.

Hypothesis #1: The fast degradation kinetics of the bimetallic Z-Loy particles will permit reactions to consume TCE at the rate it dissolves within the source zone. The net effect will be a reduction in the downgradient discharge of TCE mass.
Hypothesis #2: The ceramic core and engineered suspension of the Z-Loy product will enable the reactive particles to be well transported (minimal iron retention) within a medium 40-50 mesh Ottawa sand.
Hypothesis #3: Based upon the mass balance calculations presented in Section 2.10.1, it is hypothesized that > 50% TCE source zone mass reduction will require more Z-Loy that can be delivered to the DNAPL source (7.72 g of ZVI must be delivered to reduce 36.75 g of TCE).

3. Objectives.

While previous studies have shown promise regarding zero valent iron as means for chlorinated solvent reduction, there are still many components that must be studied. More focus must still be placed on determined the most effective surface enhancements to promote reaction and subsurface transport, as well as its ability to reduce source zones and their average mass flux downstream.

Therefore, the objectives of this study are as follows:

- Determine TCE degradation kinetics with Z-Loy in batch reactor experiments.

- Determine of the transport of Z-Loy within a medium sand using 2-dimensional aquifer cell experiments.
- Determine if Z-Loy treatment within the source zone will result in appreciable reduction of DNAPL mass.
- Determine the influence of Z-Loy treatment within the source zone on the contaminant mass discharge emanating from the source zone.

4. Batch Experiment Materials and Methods.

4.1.Chemicals.

Trichloroethylene (99.5+%) was purchased from Aldrich. Gas standards of Ethene (0.01%) and Ethane (99.5%) were provided by Alltech. 99.998% Argon and 15.0% Hydrogen were purchased from AirGas. For source zone visibility, the TCE was dyed red using Oil-Red-O (Fisher Scientific) at a concentration that has been shown not to influence the physical properties of TCE ($4x10^{-4}$ M, Ramsburg and Pennell, 2002). 0.1 N HCL, NaCl, and NaBr were provided by Fisher Scientific. Aqueous solutions were prepared with Millipore Milliq water (>18.1 MΩ-cm). Federal Fine and F-70 Ottawa sands were obtained from U.S. Silica. The Federal Fine sand was sieved to produce a 40-50 mesh Ottawa sand that was used in the experiments.

4.2.Z-Loy Suspension Preparation.

Z-Loy was donated for use in these experiments by OnMaterials, LLC. The Z-Loy material was stored in an argon. All Z-Loy suspensions were prepared within a Coy glove bag filled with argon. A trace oxygen sensor (Alpha Omega Instruments) oxygen sensor was used to monitor the concentration of O_2 within the glove bag to ensure it remained below 1000 ppm at all times. Preparation of the Z-Loy suspension followed a recipe provide by the manufacturer. In brief, 10 g of Z-Loy was mixed with 0.06 g of dispersant and added to 500 mL of

deoxygenated water to create a 1% iron suspension (Z-Loy comprises 55% iron).

4.3.Batch Reactors.

Batch tests were conducted in 120 mL serum bottles capped by Silcon/PFTE caps, with all reactor preparation conducted in an anoxic glovebox. 700 mg/L batch tests were prepared by adding 0.035 g of TCE to reactors containing the Z-Loy suspension, Z-Loy suspension and 0.1 M NaBr, and deoxygenated water alone. Reactors were then immediately capped and sealed and shaken by hand for one minute. Successive sampling was enacted, with each sample comprising 0.2 mL headspace gas. Reactors were rotated end over end at 20 rpm at 22 °C between samples.

4.4.Analytical.

Headspace samples were taken from each reactor (200 uL), and injected into an HP 5890 Series II gas chromatograph. Flow within the GC was established using nitrogen as the carrier gas and was split between two columns: GC-GASPRO column connected to a FID and a HP-MOLSIV column connected to a TCD. The samples were injected at 250 °C under splitless conditions. Oven temperature was programmed as follows: increase from 50 °C to 160 °C at 50 °C/min, remain at 160 °C for 3 minutes, increase from 160 °C to 230 °C at 25 °C/min, remain at 230 °C for 7 minutes, increase from 230 °C to 240 °C at 10 °C/min, and remain at

240 °C for 7 minutes. This method was chosen because it provided total separation between TCE and its daughter products (i.e., principally acetylene, ethene, ethane) on the FID. The TCD was used to monitor concentration of H_2. TCE standards were prepared with the same liquid to headspace ratio as the experimental reactors, while ethene and ethane standards were created on a mass basis by injecting gas standards at varying volumes into the GC. H_2 mass standards were determined using a 15% hydrogen gas standard and injecting a range of volumes into the GC. The carbon mass balance was calculated based on the initial mass of TCE added to each reactor compared with the subsequent amount of TCE and its reaction products at later observed times. Aqueous concentrations were determined based on Henry's constants found for the Z-Loy suspension. To determine these values, known masses of TCE, ethene, and ethane were injected into 120 mL serum bottles with approximately 70 mL of the Z-Loy suspension. Prior to these experiments, the Z-Loy suspension was exposed to the atmosphere and stirred for 24 hours to oxidize the iron in the suspension, yielding it unreactive. The batch reactors were then left to equilibrate over 24 hours, after which headspace samples were taken to determine the final headspace concentrations of each constituent. The Henry's coefficient for each constituent was determined with the following formula.

$$M_t = V_g C_g + V_l \frac{C_g}{K_H} \qquad (8)$$

Where M_t is the total mass in the system, V_g is the volume of the gas, C_g is the gas concentration, V_l is the volume of the liquid, and K_H is the dimensionless Henry's Coefficient.

4.5. Iron Characterization.

Fe^0 content in the Z-Loy suspension was determined by measuring the amount of H_2 produced when 20 mL HCl (0.1 N) is added to a reactor containing 1 g of the Z-Loy suspension.

$$Fe^0 + 2H^+ \rightarrow Fe^{2+} + H_2 \quad (9)$$

The 1:1 molar ratio between H_2 and Fe^0 is shown above. Reactors were rotated end over end for 24 hours, at which time the amount of H_2 produced was measured on the GC.

4.6.Reaction Rates.

Aqueous phase reaction rate constants were determined for reactors containing TCE and the Z-Loy suspension alone and TCE and the Z-Loy suspension (made with 0.1 M NaBr solution instead of deoxygenated water alone). Reaction rate constants were determined using the mathematical modeling program MATLAB

version 7.9, assuming successive reactions from TCE to ethene to ethane (with acetylene at a very low pseudo steady state), shown below.

$$\frac{dC_{TCE}}{dt} = -k_{TCE}C_{TCE} \quad (10)$$

$$\frac{dC_{Acetylene}}{dt} = k_{TCE}C_{TCE} - k_{Acetylene}C_{Acetylene} \quad (11)$$

$$\frac{dC_{Ethene}}{dt} = k_{Acetylene}C_{Acetylene} - k_{Ethene}C_{Ethene} \quad (12)$$

$$\frac{dC_{Ethane}}{dt} = k_{Ethene}C_{Ethene} \quad (13)$$

Where,

C_{TCE} is the total mass of TCE in the reactor (aqueous) in moles

$C_{Acetlyene}$ is the total mass of Acetylene in the reactor (aqueous) in moles.

C_{Ethane} is the total mass of Ethane in the reactor (aqueous) in moles.

C_{Ethane} is the total mass of Ethane in the reactor (aqueous) in moles.

k_{TCE} is the reaction rate coefficient for TCE to Acetylene (in hr^{-1})

$k_{Acetylene}$ is the reaction rate coefficient for Acetylene to Ethene (in hr^{-1})

k_{Ethene} is the reaction rate coefficient for Ethene to Ethane (in hr^{-1})

Models were developed for both successive and parallel reactions, with successive modeling yielding the better fit. For the purpose of these experiments, a direct pathway from TCE to ethene was assumed; do to the fact that no

detectable acetylene was observed in any of the experiments. The MATLAB program developed is described in the following section.

4.7. MATLAB Program.

The program is designed to analyze the degradation of TCE and production of ethene and ethane in a batch reactor. It utilizes user inputted calibration curves and known chemical properties to determine the observed mass of each component in the aqueous phase of the reactor over time (in moles). Ordinary differential equations (ODEs) (which include reaction rate coefficients(Equations 1-4 above)) with known initial conditions are then solved and compared to the observed data. The initial conditions (C_{TCE}, C_{Ethane}, and C_{Ethane}) were the initial aqueous moles of TCE in the reactor, zero, and zero, respectively. Reaction rate coefficients were simultaneously adjusted to yield the best fit of the ODE reaction model to the observed data (minimizing the sum of the squares of the residuals). Residuals of the observations based on the model and percent of total mass conserved at each observation (sum of gaseous and aqueous phases of each component) are shown in Section 5.1.

4.8.Aquifer Cell Studies.

Aquifer cell experiments were conducted to assess the transport and reaction of Z-Loy within a TCE-DNAPL source zone. The aquifer cell has dimensions of 63.5

cm x 38 cm x 1.4 cm with 18 screw cap sampling ports in four vertical sections to determine local concentrations throughout the box (Figure 2).

The cell was packed under water saturated conditions with a 2 inch layer of F-70 Ottawa sand at the bottom. The remainder of the box was packed using 40-50 mesh Ottawa sand as the background medium and F-70 Ottawa sand for lower permeability lenses. Lower permeability lenses were placed an inch above the bottom F-70 layer and directly below the source zone injection needle (Figure 2).

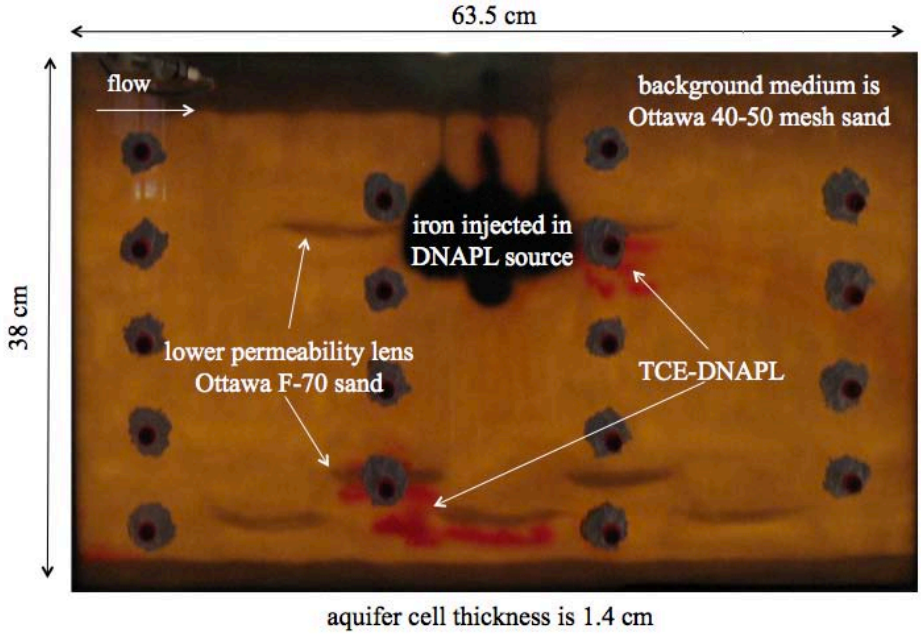

Figure 2. Aquifer Cell Schematic

Upon completion of packing, a 2.5 pore volume (with 0.33 pore volume pulse) tracer test (0.1 M NaCl) was conducted at a flow rate of 4.5 mL/min. Next, approximately 25-30 mL of dyed TCE was injected into the source zone at 0.5 mL using a syringe pump fitted with an 18-gauge needle that ended 15 cm below the surface in the center of the cell. The TCE was allowed to redistribute over 24

hours. Another post injection NaCl tracer test was conducted over 2.5 pore volumes (with 0.33 pore volume pulse). Influent and effluent solutions were transferred through 2 fully screened aluminum rectangular chambers (1.27 cm x 1.27 cm) located on both ends of the aquifer cell. Each end-chamber was milled to contain 0.203 mm slits along the length of the chamber to produce a well screen. A constant head reservoir located at the influent end of the cell controlled the flow through the box. The Z-Loy suspension was injected either upgradient of the source zone or directly into the source zone (Experiment A and B, respectively) at 5 mL/min (background box flow of 1 mL/min) using a steady flow syringe pump. Successive 0.5 mL port and 0.5 mL effluent samples were taken downstream of the source zone. Samples were extracted from the box ports/effluent chamber were analyzed using a Perkin Elmer Turbomatrix 40 Trap Autosampler connected to the GC described above. The autosampler settings were as follows: the needle temperature was 120 °C, the transfer line temperature was 130 °C, the vial oven temperature was 90 °C, and the injection and column pressures were both 25 psi. Calibration curves for TCE, ethene, and ethane were created with the same liquid/headspace volume ratio containing ranging concentrations of the constituents. TCE-DNAPL saturations were determined using a light transmission system comprising a Flathead 80 light bank and a Nikon Coolpix 950 digital camera, with saturations determined based upon the hue in the image (Suchomel and Pennell, 2006). In brief, thickness averaged saturations were determined on a pixel basis using a MATLAB script developed by Suchomel and Pennell (2006). The ganglia-to-pool (GTP) ratios of the

saturation distributions (ratio of volume in the cell at saturations lower than the residual saturation to the volume greater than residual saturation) were determined using the DBA(discrete block approach) and CBA(continuum based approach) averaging approach (Christ et al. 2011).

5. Results and Discussion.

5.1. Batch Reactivity.

Batch studies were conducted to determine the reactivity of Z-Loy under iron limiting conditions to ensure that all available iron is reacted (although under TCE limiting conditions, surface deactivation is minimized). Over the course of this study, three different lots of Z-Loy were used. Out of these three lots, the second lot was determined to be non-reactive with TCE (data not discussed further below), with the other two producing similar results. In addition, the ionic effects of 0.1 M NaBr and NaCl on reactivity were analyzed. A summary of all batch experiments is shown in Table 3.

Table 3. Summary of kinetic batch experiments (T=22±2 °C)

Reactor	R1	R2	R3	R4	R5	R6	R7
Reactor volume (mL)	124	121	122	124	122	123	122
Liquid volume (mL)	71	68	74	74	72	72	72
Headspace volume (mL)	53	53	48	50	50	21	21
Mass TCE (umol)	647	586	266	236	206	213	160
TCE initial headspace concentration (uM)	2420	2269	982	863	769	894	598
TCE initial liquid concentration (uM)	7304	6849	2963	2605	2320	2699	1804
Z-Loy solids loading (g/L)	22	20	21	22	21	23	21
Z-Loy solids specific surface area (m^2/g)	1	1	1	1	1	1	1
Z-Loy shipment identifier	I	I	III	III	III	III	III
Cl^- concentration (uM)	0	0	0	0	0	0	100
Br^- concentration (uM)	0	0	0	0	110	110	0
k_1 (1/hr)	0.001670	0.001118	0.006956	0.012049	0.005800	0.004893	0.013549
k_2 (1/hr)	0.000049	0.000076	0.000329	0.000353	0.000219	0.000256	0.000090
k_{H2} (mmol/hr)	0.07200	0.07050	0.06450	0.07190	n/a	n/a	n/a
k_1 (L/g-hr)	0.000154	0.000103	0.000642	0.001112	0.000535	0.000452	0.001251
k_2 (L/g-hr)	0.000005	0.000007	0.000030	0.000033	0.000020	0.000024	0.000008
k_{H2} (L-mmol/g-hr)	0.00647	0.00641	0.00586	0.00654	n/a	n/a	n/a
k_1 (L/m^2-hr)	0.000154	0.000103	0.000642	0.001112	0.000535	0.000452	0.001251
k_2 (L/ m^2-hr)	0.000005	0.000007	0.000030	0.000033	0.000020	0.000024	0.000008
k_{H2} (L-mmol/ m^2-hr)	0.00647	0.00641	0.00586	0.00654	n/a	n/a	n/a

Daughter products of the reactive Z-Loy lots consisted of even number saturated alkenes (ethene and ethane). It was determined that ethene was a reactive intermediate which was converted to ethane and both ethene and ethane were the observed in the batch reactors at experiments end. In all cases, amounts of other daughter products were negligible. Therefore, the kinetics were modeled assuming a direct pathway to ethene, followed by a pathway from ethene to ethane (Elliot and Zhang, 2001) (see Equations 1-4 in Section 4.6). Fitted rate coefficients were found for the gas phase of each constituent, which were then converted to aqueous phase rate coefficients through dimensionless Henry's coefficients of 0.63, 11.42, 1.39 for TCE, ethene, and ethane, respectively. Fitted aqueous rate coefficients for the first and third lots of Z-Loy are shown in Table 3. The average, surface area normalized, pseudo-first-order rate coefficient (found in MATLAB model) for the consumption of TCE (k_1) was found to be $(8.77 \pm 0.15) \times 10^{-4}$ L/m^2-hr ($(8.77 \pm 0.15) \times 10^{-4}$ L/g-hr). These surface area normalized values are comparable to many polymer coated iron particles shown previously in Table 1. The daughter products observed were similar to those found for bimetallics (ethene and ethane). It should be noted that the behavior of both lots yielded similar results, demonstrating consistent manufacturing. Figures 3-4 shows a representative analysis of the four batch experiments conducted without salts.

NaBr was intended to be a background electrolyte in the aquifer cell experiments (with NaCl as a tracer), so batch experiments were conducted with 0.1 M NaBr

and NaCl aqueous solutions to determine if it presents significant effects on Z-Loy reactivity. Figure 5 shows this data from three batch experiments and the fits obtained by adjusting the two rate coefficients. Table 3 also shows the surface normalized, pseudo first order reaction rate constants for TCE to ethene to ethane, and the observed reaction rate constant when Z-Loy is used in the presence of 0.1M NaBr and NaCl.

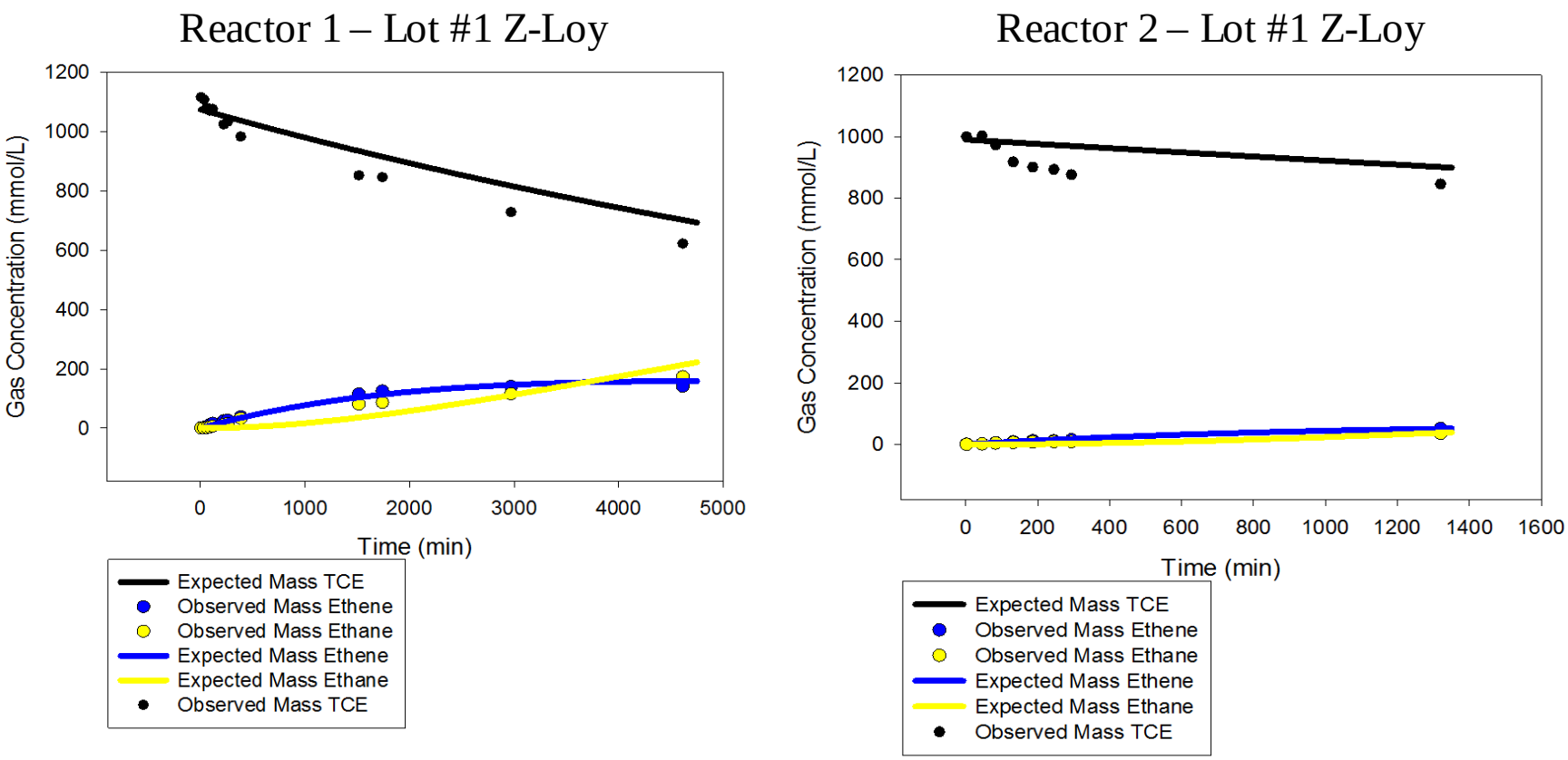

Figure 3. Batch data and expected model fits for the reaction of TCE with Z-Loy: Z-Loy Shipment I in Milli-Q water

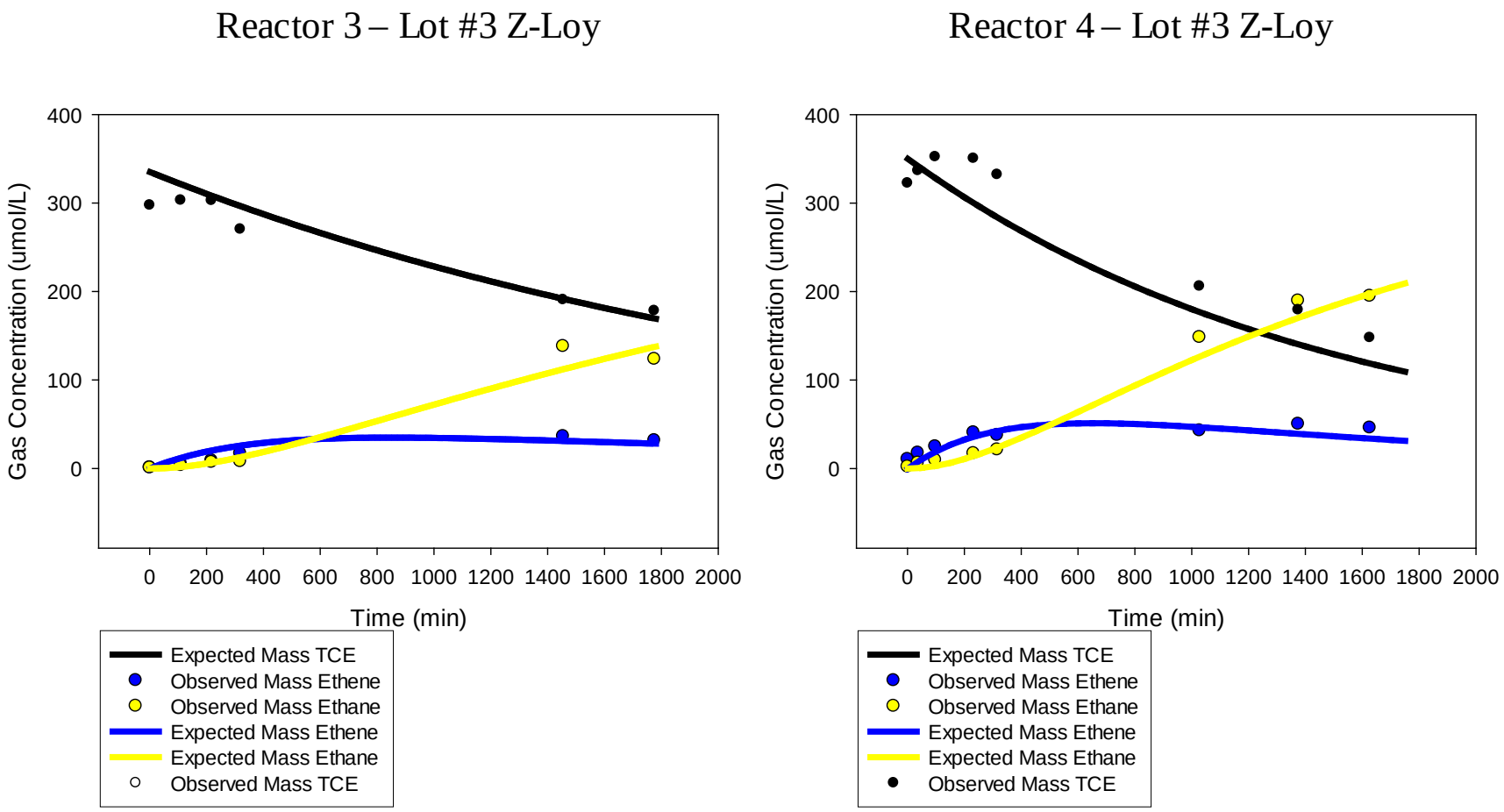

Figure 4. Batch data and expected model fits for the reaction of TCE with Z-Loy: Z-Loy shipment III in Milli-Q water

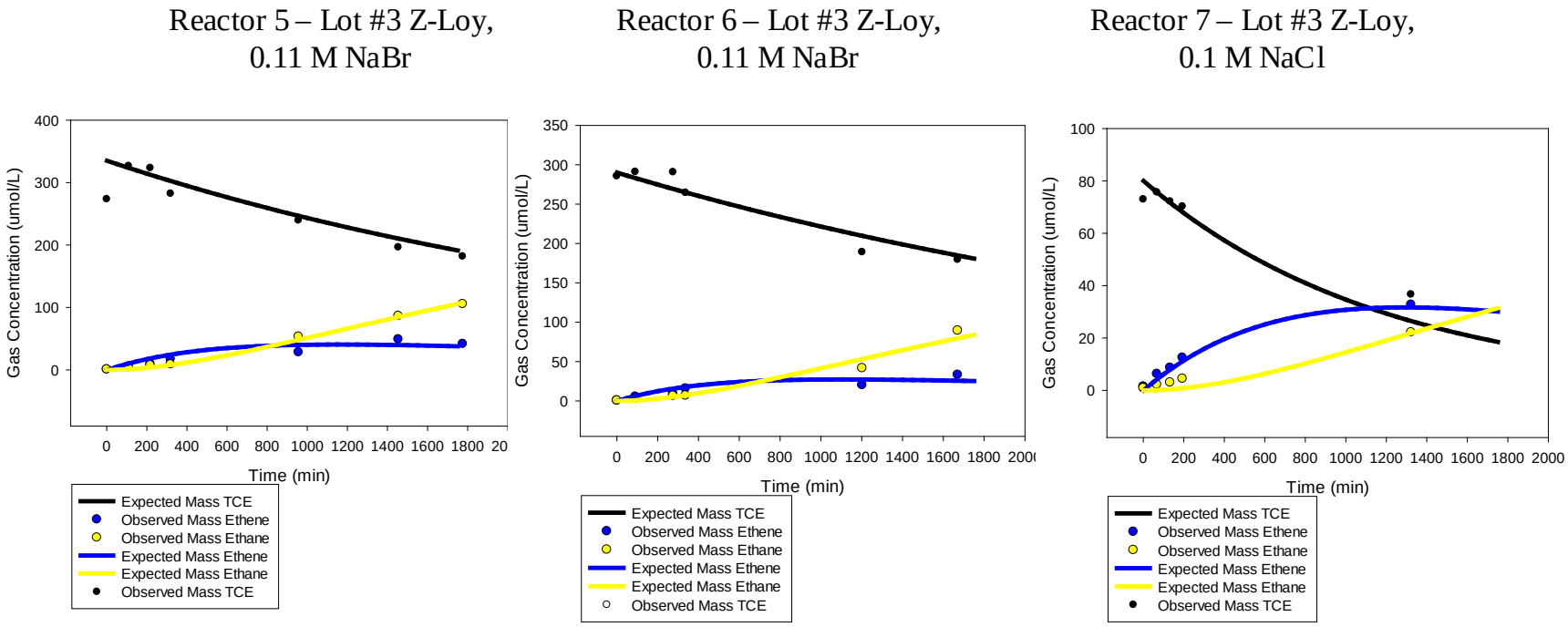

Figure 5. Batch data and expected model fits for the reaction of TCE with Z-Loy: Z-Loy in 0.11 M NaBr and 0.10 M NaCl.

For batch experiments containing 0.1 M NaBr, almost every k_2 was reduced. It was determined that the box would be run without NaBr as a background electrolyte.

Hydrogen production was also observed over the course of the batch experiments. The production of H_2 for Z-Loy was zeroth order between approximately 500 and 1500 minutes, and was zero at all other times.

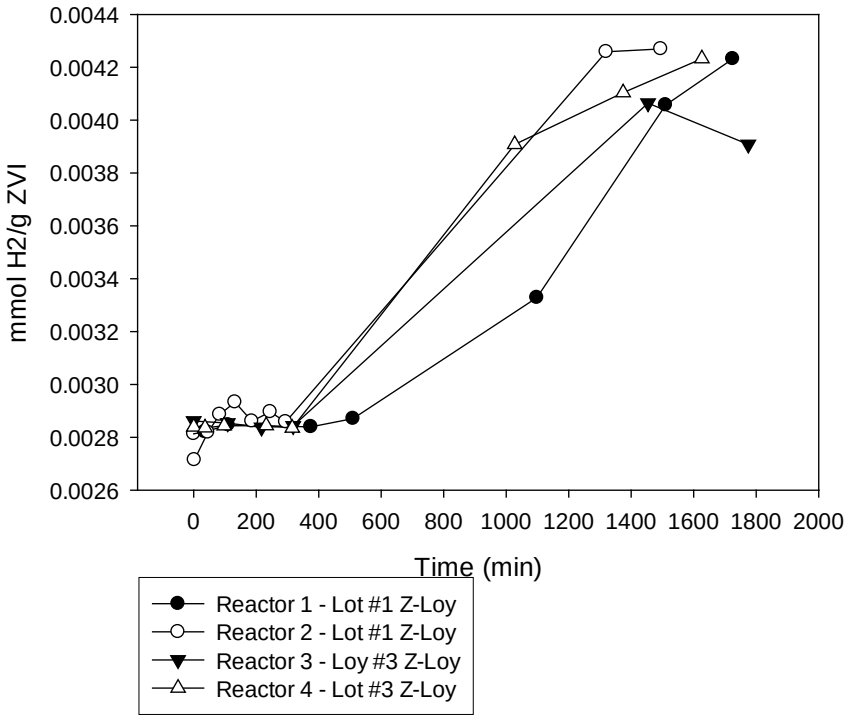

Figure 6. Hydrogen Production in Batch Reactors 1-4 (described above)

There was negligible H_2 production for batch reactors containing the 0.1 M NaBr and 0.1 M NaCl solution. Due to the lower masses of H_2 observed, it is unlikely that the Z-Loy provided for this study was not bimetallic (hydrogenation catalyst).

Finally, it was determined that H_2 production did not affect TCE reduction kinetics.

Initial and final pH values were observed in all batch experiments. In all cases, the initial pH was approximately 8.5 and the final was approximately 8.9 to 9. This suggests the consumption of H^+ (the iron acts as an H^+ scavenger to produce H_2) increases the pH, though this pH increase is mitigated by the hydrogenolysis reaction which consumes TCE - a reaction which decreases pH.

5.2. *Aquifer Cell Experiments.*

Two aquifer cell tests were conducted to determine the transport, source zone reduction ability, and average mass flux reduction capabilities of Z-Loy. Shown in Table 5 are important properties related to each aquifer cell experiment.

Table 4. Aquifer Cell Properties

	Experiment A	Experiment B
Background Material	40-50 Ottawa Sand	40-50 Ottawa Sand
Low Permeability Lens Material	F-70 Ottawa Sand	F-70 Ottawa Sand
Pore Volume (mL)	1364	1312
Expected Flow Rate (mL/min)	4.50	4.50
Residence Time (hr)	4.86	4.86
Volume TCE Added (mL)	31.81	23.29
Overall NAPL Saturation	2.33%	1.75%
GTP Ratio (pixel basis)	0.110	0.094
GTP (with DBA (discrete block approach))	0.181	0.162
GTP (with CBA(continuum based approach))	0.182	0.162
Overall Hydraulic Conductivity (cm/min)	4.30	3.58
Z-Loy Added (mL)	204	391

For both aquifer cells, four ports downstream of the source zone were monitored. These ports were chosen to focus on the upper portion of the source zone (Figure 7). Port 1 was chosen to monitor the dissolved concentrations immediately downstream of the source zone. Port 2 was chosen to monitor vertical displacement and transport. Ports 3 and 4 were chosen to further describe the average mass flux out of the upper half of the source zone.

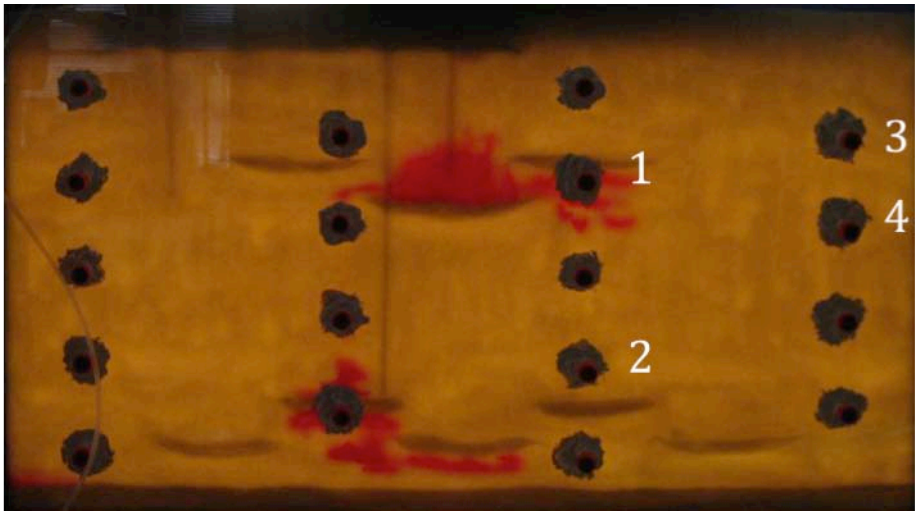

Figure 7. Side port sampling locations in Experiments A and B.

5.2.1. Experiment A – Z-Loy Transport though a TCE-DNAPL source.

This experiment was designed to assess transport through a DNAPL source zone. Subsequent to the post NAPL injection tracer test, 200 mL of Z-Loy suspension was injected through the needle upstream of the source zone at a rate of 5.0 mL/min. This explores Z-Loy's potential to be transported to a source zone from locations upgradient. Background flow in the box during the Z-Loy injection was 1.0 mL/min. Upon completion of injection of Z-Loy, the background flow was

increased to 4.5 mL/min and remained at that rate for the duration of the experiment. Port and effluent samples were analyzed for TCE, acetylene, ethene, and ethane. In addition, Cl^- production and total iron was monitored in effluent samples. The resulting port sample data and flux-averaged effluent data are shown in Figures 8 and 9. Observations though the course of the experiment suggest that the Z-Loy did not transport within the medium sand.

Moreover no iron was detected in the effluent samples. This lack of detectable quantities of iron in the effluent samples confirms that the Z-Loy particles were immobilized upgradient of the source zone.

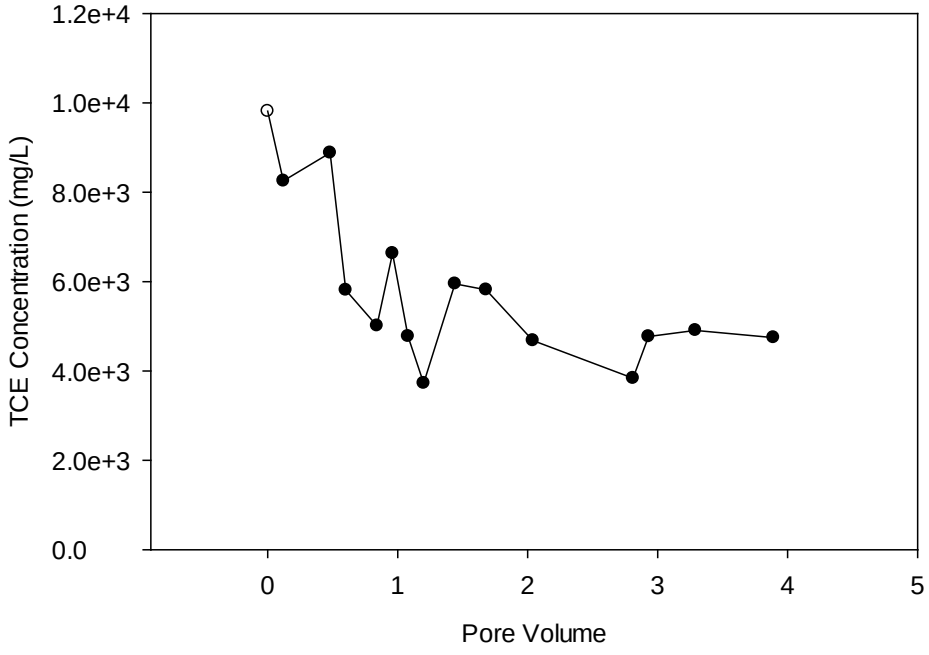

Figure 8. TCE Effluent Data (Aquifer Cell #1)

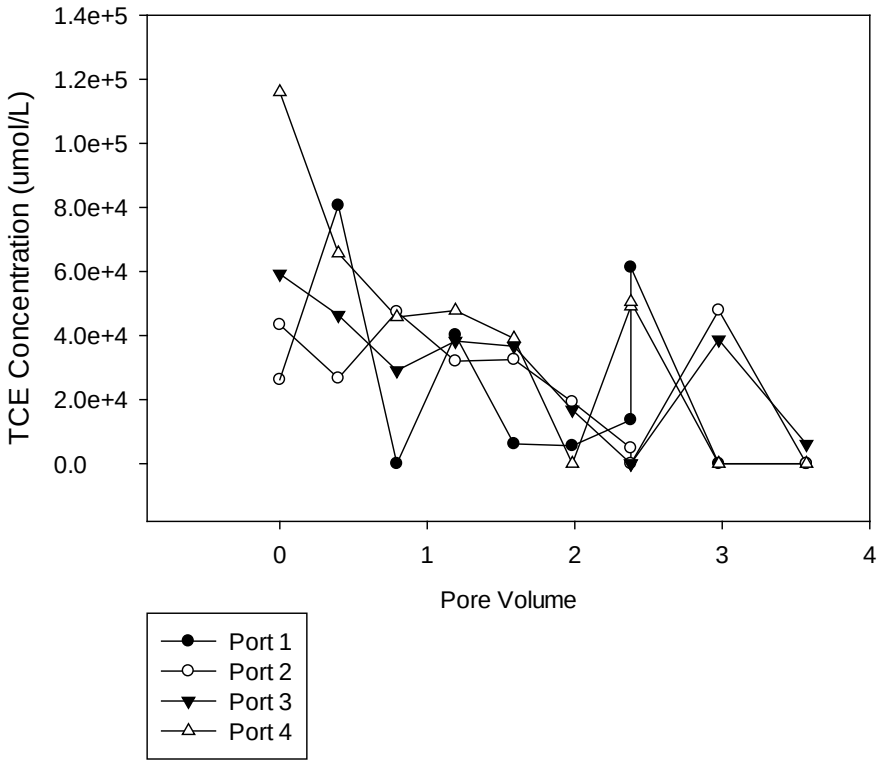

Figure 9. TCE Port Data (Aquifer Cell #1)

In all samples, negligible amounts of ethene and ethane were observed (i.e., the highest measured concentration of ethene or ethane was approximately 10 μM). Additionally, production of H_2 and Cl^- was not quantifiable. TCE concentrations, however, decrease in both the ports downstream of the injection location and in the effluent samples. Subsequent to the Experiment A, an additional set of batch experiments were conducted using the same shipment of Z-Loy. These tests showed that the Z-Loy product was minimally reactive with TCE. Thus, Experiment A represents an opportunity to assess the transport of the Z-Loy material in the absence of gas production and reaction. Under these conditions, the reductions in TCE concentrations observed in both the effluent and side port

samples are hypothesized to result from changes to the flow field created by the injection of the Z-Loy mass.

To explore this hypothesis further, a tracer test conducted after the injection of Z-Loy was compared to tracer test data collected after the introduction of NAPL (Figure 10).

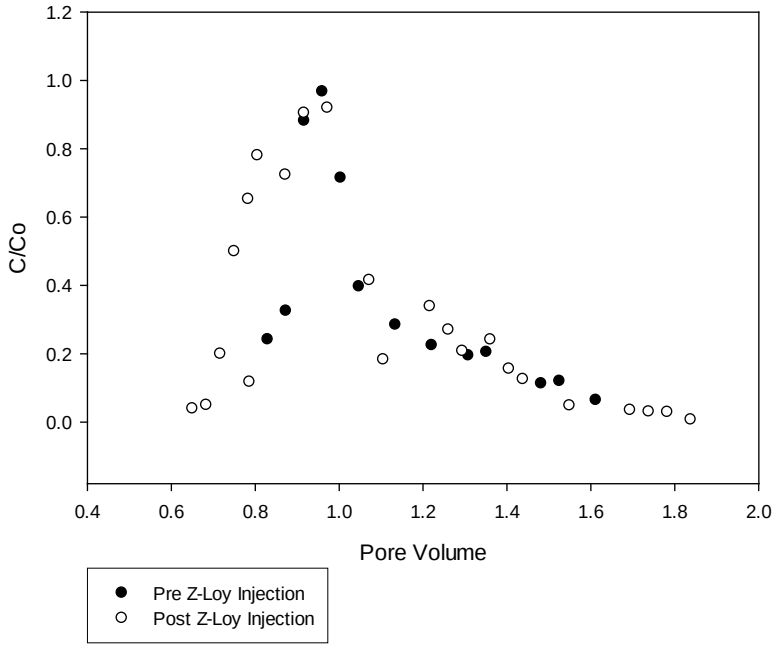

Figure 10. Aquifer Cell #1 Tracer Tests (Pre and Post Z-Loy Injection)

The tracer conducted following Z-Loy injection broke through about 25% earlier than the TT conducted prior to injection, supporting the hypothesis of flow alterations caused by pore clogging. Additionally, a moment analysis was conducted and the mean residence time pre-injection was 0.704 pore volumes, compared to post-injection, which was 0.569 pore volumes.

It should be acknowledged that the Erioglaucine A dye used in this study is organic, and has the possibility to react with iron particles as well as the NAPL. As shown in figures 11 through 13, it becomes clear that the Erioglaucine dyed influent flow is reacting with the iron particles (as shown in the reduction in color).

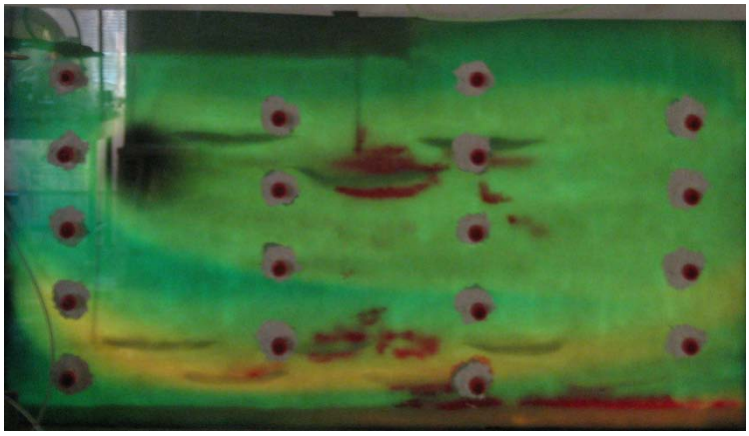

Figure 11. Aquifer Cell #1: During Final Z-Loy Injection

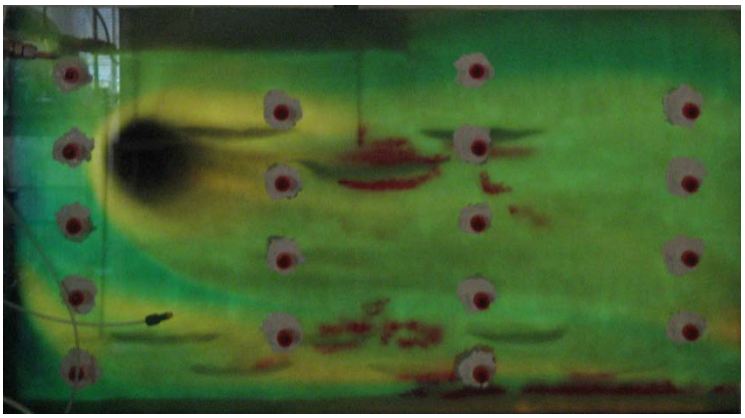

Figure 12. Aquifer Cell #1: 0.25 Pore Volumes After Final Z-Loy Injection

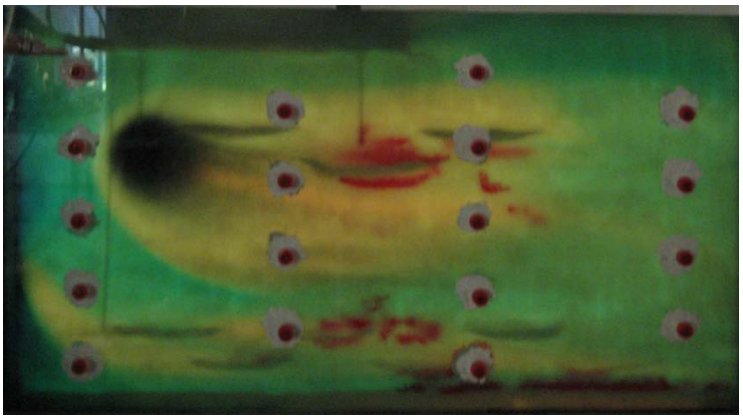

Figure 13. Aquifer Cell #1: 0.75 Pore Volumes After Final Z-Loy Injection

Therefore, batch tests were conducted to determine the extent in which the dye reacts with the iron particles. The reactors were setup in the same manner as the reactivity studies, yet included Eriogluacine A and did not include TCE. In these experiments the production of H_2 was monitored as an overall measure of reactivity. Over the course of the experiment, H_2 mass rapidly increased then slowed after approximately 5 hours as shown in Figure 14. The dye acts as a catalyst for hydrogen production with the iron, while the reactor with the dye alone has minimal to no hydrogen production due to lack of a reaction.

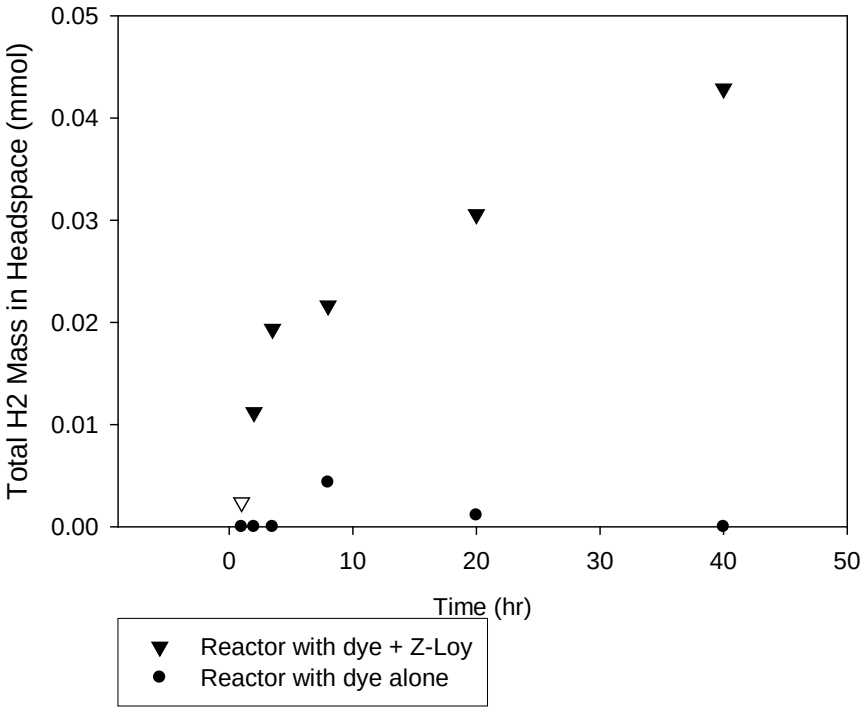

Figure 14. H_2 Production in Reactor Containing Z-Loy and 0.021 mM Erioglaucine A

It was also observed that at the end of the experiment, no visible blue hue was detectable in the reactor containing Z-Loy, further proving a reaction and explaining the reduction in color in the flow downstream of where the dye and particles meet. Note however, that the Erioglaucine A dye did not preclude the TCE reaction. As described above, batch tests conducted with this batch of Z-Loy in the absence of Erioglaucine A suggest that the batch had limited reactivity with TCE (as the Z-Loy reacts with the dye). In fact, further batch data suggest Erioglaucine A increases hydrogen production. Here a destructive sampling

routine was conducted on five reactors over 24 hours. For each reactor, 50 ml of the Z-Loy suspension was added. Over the course of the next 24 hours, reactors were sampled for H_2 mass. After a reactor was sampled, 50 mL of 2x concentrated dyed Erioglaucine solution were injected. One minute later, the H_2 mass was again measured. Results of these experiments are shown in Figure 15. In all cases the introduction of Erioglaucine A resulted in a dramatic increase in the production of H_2 (Figure 15).

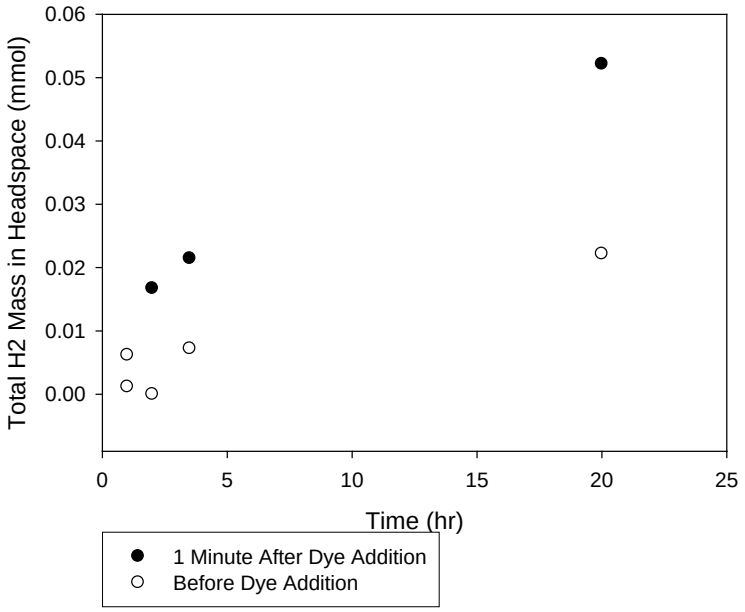

Figure 15. H_2 Production in Reactors Before and After Addition of Erioglaucine

Given these observations that indicate the dye is interacting with the iron particles, it was determined that the second aquifer cell would be conducted without dye.

5.2.2. Experiment B - Injection within a DNAPL-Source

A second aquifer cell study was conducted with a new supply of Z-Loy that was determined to be reactive (see batch results in Section 5.1). In this experiment Z-Loy was injected directly into the NAPL source zone. Tracer tests were conducted using the procedures described in Section 5.2.1 before and after the spill of approximately 23 mL of TCE-DNAPL (dyed red). Subsequent to the second (i.e., post-DNAPL spill) tracer test, 200 mL of Z-Loy was injected directly into the NAPL at 4.5 mL/min using an 18-gauge needle. Clogging of the 18 gauge injection needle necessitated its replacement by a 1/8 inch tube. The background flow during the Z-Loy injection was 1.0 mL/min. Flow continued at 4.5 mL/min for 1.5 pore volumes after the end of the Z-Loy injection, before an additional 100 mL of Z-Loy was injected on each side of the previous injection. These secondary injections were used to fully encapsulate the upper portion of the TCE-NAPL source. The injections were conducted sequentially (right then left) using the same procedure used for the first injection (5.0 mL/min) injection rate under 1.0 mL/min background flow. Background flow was continued at 4.5 mL/min for the next three pore volumes before the first of four flow interruptions was initiated. Subsequent flow interruption occurred at 4.5, 6, and 7.5 pore volumes (flow occurred at 4.5 mL/min after all flow interruptions). Port and effluent samples were analyzed for TCE, acetylene, ethene, and ethane. In addition, Cl^- production and total iron were monitored in effluent samples.

Figures 16 and 17 show the observed flux-averaged effluent concentrations of TCE and ethene and ethane, respectively. Figures 18 through 21 show the observed port concentrations of TCE, ethene and ethane, respectively.

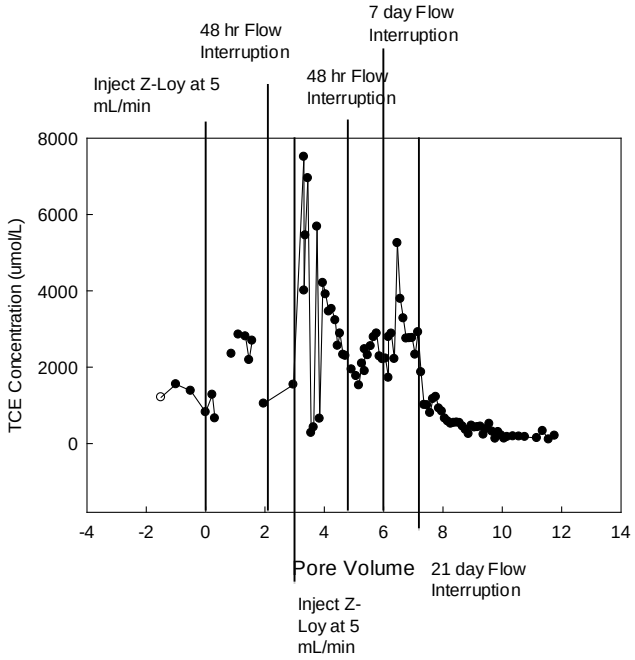

Figure 17. Effluent TCE Concentration (Aquifer Cell #2)

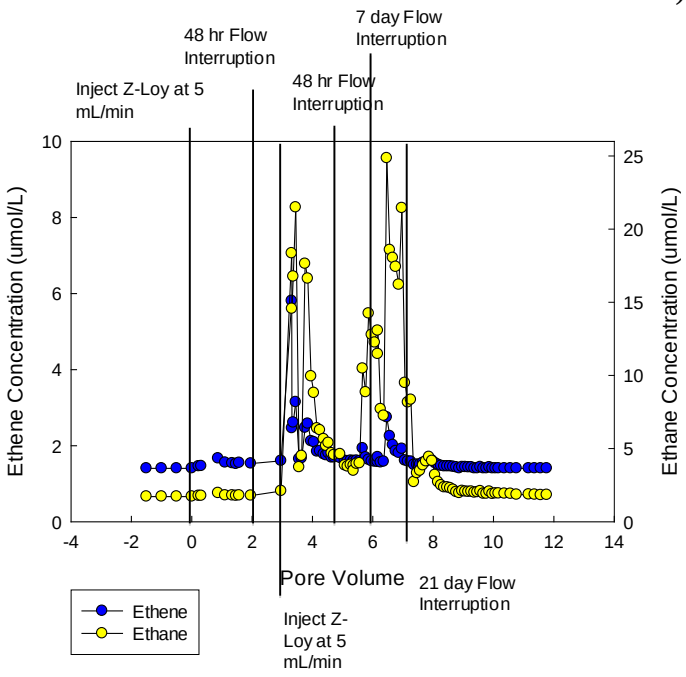

Figure 17. Effluent Ethene and Ethane Concentration (Aquifer Cell #2)

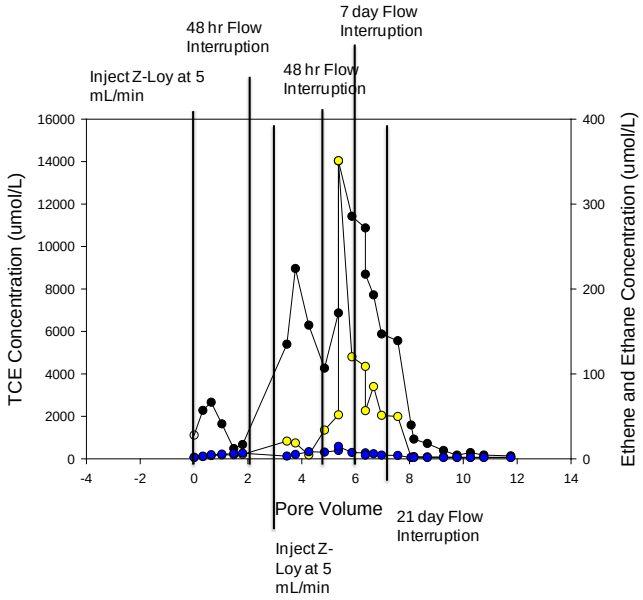

Figure 18. Port 1 Concentrations (Aquifer Cell #2)

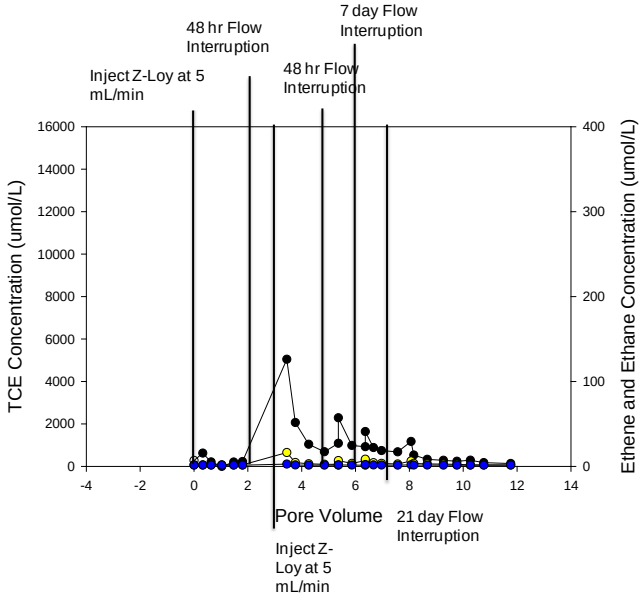

Figure 19. Port 2 Concentrations (Aquifer Cell #2)

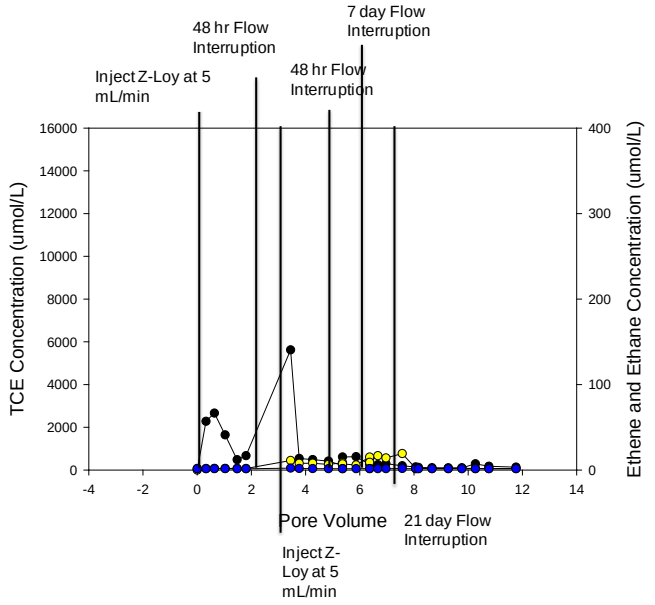

Figure 20. Port 3 Concentrations (Aquifer Cell #2)

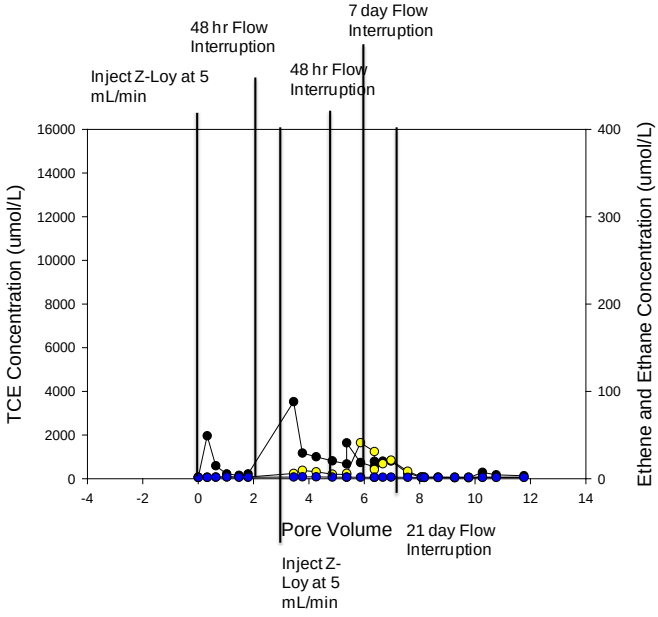

Figure 21. Port 4 Concentrations (Aquifer Cell #2)

Port 1, which is directly downstream of the source zone, showed greatest amounts of TCE and daughter products. Ports 3 and 4 showed an increase in concentrations following injection, but the concentrations were not of the same magnitude as Port 1. Port 2 also showed the greatest relative increase in concentrations

following the second set of injections. This increase is consistent with the influence of TCE-NAPL mobilization. All of flow interruption occurrences within the first 8 pore volumes were followed by increases in concentrations of all constituents in both port and effluent samples. The size of the increase was proportional to the duration of flow interruption in all port and effluent sampling, indicating that the Z-Loy suspension is partitioning into the TCE source zone. When flow interruptions occurred many days following injection, increases in ethene and ethane were also large, suggesting that reaction is still occurring. Following the final flow interruption, concentrations of TCE, ethene, and ethane all decreased in similar patterns. This indicates that the reactive capacity of the iron is exhausted or very near exhaustion. Subsequent decreases in TCE concentration in the ports may be due to flow field alterations given that the approximately 400 mL of Z-Loy injected represented approximately 22.40 reducing milliequivalents (i.e., maximum of 2 mL of TCE reacted).

The effective reaction rate coefficients within the source zone were then determined and compared to the reaction rate coefficients found in batch studies. To do this, a simple plug flow with dispersion reactor model was applied.

$$\frac{C_{out}}{C_{in}} = \frac{4a\exp\left[Pe\frac{(1-a)}{2}\right]}{(1+a)^2-(1-a)^2\exp(-aPe)} \qquad (14)$$

Where, C_{out} is the concentration leaving the reactive zone, C_{in} is the concentration entering the reactive zone (solubility of TCE), $a = \sqrt{1 + \frac{4k\bar{t}}{Pe}}$ (k is the effective rate coefficient (the net rate for the system where dissolution is occurring within the reactive zone), $\bar{t}$ is the mean residence time, and $Pe = \frac{Lv}{D}$ (L is a characteristic length, v is the fluid velocity, and D is the diffusivity)). To yield the most accurate representation of source zone reduction, C_{out} values were taken from Port 1 samples (closest to the Z-Loy injection area and TCE source zone) and were well after flow interruptions to eliminate Z-Loy/NAPL partitioning effects. A characteristic length of 0.152 meters was chosen (the width of the reactive zone in the aquifer cell), as well as a typical diffusivity of 1×10^{-9} m^2/s. The effective reaction rate coefficient found was 8.18×10^{-5} L/m^2-hr (8.18×10^{-5} L/g-hr). This value is about an order of magnitude less than those found for the batch reactors ($(8.77 \pm 0.15) \times 10^{-4}$ L/m^2-hr ($(8.77 \pm 0.15) \times 10^{-4}$ L/g-hr)). This result is consistent with previous studies that show reduced relativities of iron particles within the source zone.

The observation of limited iron transport within the box permits estimation of the mass and concentration of iron within the source zone. These were estimated to be 8.80 g and 21.70 g/L, respectively, using a visual assessment of the impacted area, box width and initial porosity. Light transmission data suggest that the mass of TCE was 18.19 g. Thus, the Fe^0 to DNAPL mass ratio was 0.02:1 which

compares poorly to the stoichiometric amount of iron need to treat a given mass of TCE-DNAPL (0.42:1).

Effluent samples were taken to monitor for potential Cl^- concentrations. The Cl^- concentration increased over the first 3 pore volumes, and gradually decreased as the Z-Loy stopped reacting with the source zone as shown in Figure 19. This is indicative of the reduction of TCE and can be used to estimate the total mass of TCE degraded. Shown in Figure 19 are several measures of the mass of TCE-DNAPL that was treated (i.e., recovered and reacted). The data in Figure 23 suggest dissolution is the dominant treatment mechanism in Experiment B. Overall reaction and dissolution reduced the source mass by 18% (4.48 g). The inactivation of the iron can be seen through the plataued recovery curves in Figure 23.

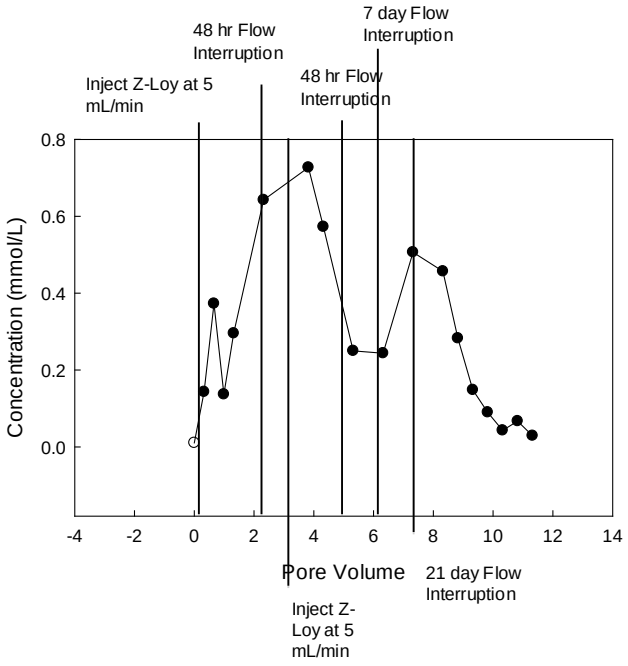

Figure 22. Cl^- Effluent Concentration (Aquifer Cell #2)

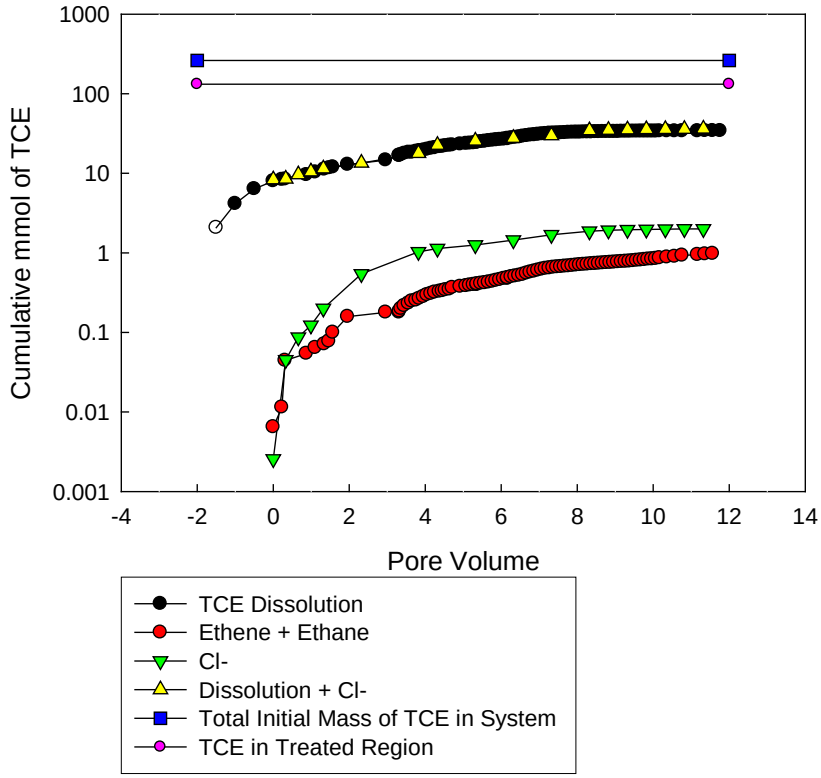

Figure 23. Recovery and transformation of TCE in Aquifer Cell #2 (Negative Pore Volumes are Prior to Z-Loy Injection)

The mass of TCE reacted was far less. Estimates based upon the chloride produced suggest 0.266 g of TCE were reacted (assumes complete conversion). Following completion of aquifer cell sampling, the light transmission analysis yielded a remaining DNAPL volume of 10.1 mL, excluding the volume of the box containing the iron. Recall that the initial DNAPL volume was 23.3 mL, with ~14 mL estimated to ride within the treated zone. The estimated initial mass in the treated zone was 18.19 g.

Finally, the cumulative equivalents of TCE reduced based on the amount of ethene + ethane, and Cl^- observed were determined to be 2.00 mmol. The discrepancy between moles of Cl^- and ethene + ethane may be explained by gas escape through the top of the aquifer cell or that there are reaction products not accounted for in this study. Overall, the combined results shown in Figures 14 and 20 suggest the reduction in source zone mass and mass discharge may be attributable to dissolution and flow field alterations, and not the reaction (i.e., reaction accounted for 5.88% mass removal).

As was the case in Experiment A, effluent data from Experiment B did not contain detectable quantities of iron suggesting limited mobility of Z-Loy within the box (which matched the visual assessment of limited transport of Z-Loy within the source zone). The influence of the Z-Loy injection on the flow field was assessed using a third tracer test (Figure 24). Additionally, a moment analysis was again conducted and the mean residence time pre-injection was 0.823 pore volumes, compared to post-injection, which was 0.693 pore volumes. Tracer data for pre and post-Z-Loy injection are shown below in Figure 23.

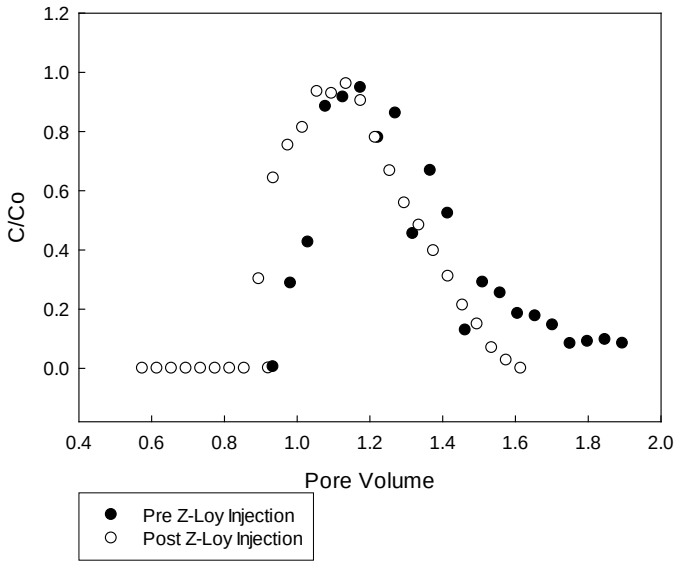

Figure 24. Aquifer Cell #2 Tracer Tests (Pre and Post Z-Loy Injection)

The flow field was further explored using a dyed tracer following the completion of the Experiment B. Images of this dye tracer flush elucidate the flow field alteration and are shown in shown in Figures 25 through 28.

Figure 25. Aquifer Cell #2: 0.2 Pore Volumes of Dyed Tracer Introduction

Figure 26. Aquifer Cell #2: 0.35 Pore Volumes of Dyed Tracer Introduction

Figure 27. Aquifer Cell #2: 0.5 Pore Volumes of Dyed Tracer Introduction

Figure 28. Aquifer Cell #2: 0.75 Pore Volumes of Dyed Tracer Introduction

The influence of the Z-Loy injection process on DNAPL mobility was examined using light transmission data. The injected iron prohibits interrogation of the DNAPL within the injected zone. Thus the assessment of DNAPL mobilization was made based upon the DNAPL located in the lower half of the box. As can be seen in Figures 29-32 the saturations at the lower half of the box remain relatively similar suggesting that large quantities of TCE-DNAPL did not drain if mobilized.

Figure 29. Source Zone, Pre Z-Loy

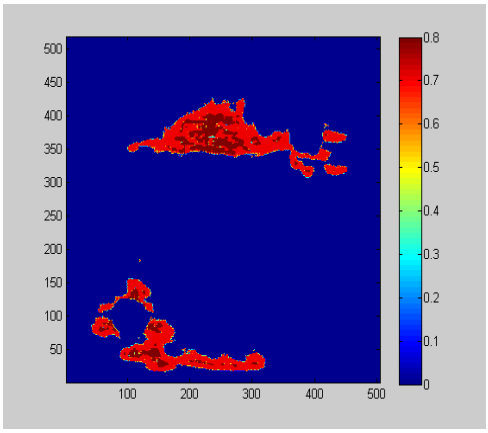

Figure 30. Source Zone Saturation, Pre Z-Loy

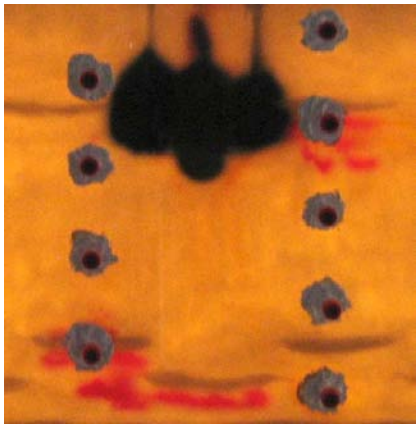

Figure 31. Source Zone, Post Z-Loy

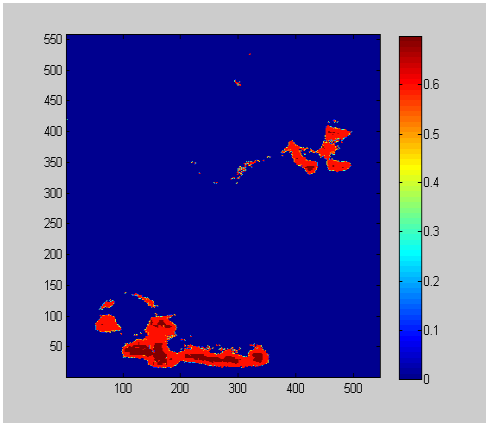

Figure 32. Source Zone Saturation, Post Z-Loy

Clearly, while some reaction was occurring between the NAPL and Z-Loy, it did not account for the majority of the decrease in port and effluent concentrations. This reduction is most likely due to the effects of dissolution and an altered flow field.

6. Conclusions

Results from batch and aquifer cell experiments suggest that Z-Loy has limited ability to reduce TCE source zones. Using the concentration of Z-Loy recommended by the manufacturer and maximizing the rate of reaction by assuming that the aqueous phase concentration is fixed at the solubility of TCE in water suggests Z-Loy can reduce approximately 30 % of NAPL saturation. Batch experiments showed ethene and ethane to be the daughter products produced with pseudo first order rate coefficients comparable to those found for bimetallic particles (Elliot and Zhang, 2001), yet the lack of H_2 production indicates a lack of a hydrogenation catalyst. It should be mentioned that OnMaterials donated the Z-Loy particles to this study, and therefore, there was little control over which lots were delivered. However, the ability to tailor the particle characteristics (i.e. surface area, metal catalyst) can help significantly.

While these batch tests suggest approximately 30% reduction at saturation, 2-dimensional aquifer cell tests suggest only limited reduction in both the source zone and average mass flux. This is likely due to very limited iron particle transport and pore clogging, leading to inaccessible reactive sites (Phenrat et al., 2007; Tratnyek and Johnson, 2006). Therefore, the reduction in source zone mass is due primarily to dissolution (4.48 g) and reduction in port and effluent concentrations is due to a reduced flow field.

While Z-Loy is not highly effective at reducing NAPL source zone mass, it may be effective if implemented downgradient of the source zone. The limited

transport of the Z-Loy observed in the aquifer cell experiments along with the inability of the dechlorination reaction to keep up with the rate of dissolution suggests Z-Loy may be best implemented in a manner that forms a zone of relatively stationary iron particles, much like a PRB. This type of implementation may be more effective at reducing TCE concentrations emanating from DNAPL source zones.

Additionally, such particles merit further investigation should better particle encapsulation be developed, leading to better transport and reactivity. Some possible areas of examination are to characterize flow fields at sites where iron is being considered for use, and then reassessing the flow after the iron injection. Furthermore, it may prove helpful to core the treated zones at sites to assess the distribution of iron. In brief, Z-Loy particles show promise in their ability to reduce NAPL source zones should further examinations continue.

References.

Arnold, WA and AL Roberts. 2000. Pathways and Kinetics of Chlorinated Ethylene and Chlorinated Acetylene Reaction with Fe(0) Particles. Environ. Sci. Technol. 34 (9).1794–1805.

Berge, N.D. and C.A. Ramsburg. 2009. Oil-in-Water Emulsions for Encapsulated Delivery of Reactive Iron Particles. Environmental Science & Technology. 43. 13. 5060-5066.

Berge, N. D and C.A Ramsburg. 2010. Iron-mediated trichloroethene reduction within nonaqueous phase liquid. J. Contam. Hydrol. 118(3-4). 105-116.

Cho, Y. and S. Choi. 2010. Degradation of PCE, TCE and 1,1,1-TCA by nanosized FePd bimetallic particles under various experimental conditions. Chemosphere. 81(7). 940-945.

Cushing, B. L., V.L. Kolesnichenko, and C.J O'Connor. 2004. Recent advances in the liquid-phase syntheses of inorganic nanoparticles. Chem. Rev. 104. 3893–3946.

Devlin, J. F. and K.O. Allin. 2005. Major anion effects on the kinetics and reactivity of granular iron in glass-encased magnet batch reactor experiments. Environ. Sci. Technol. 39. 1868−1874.

Elliott, D. W., W.-X Zhang. 2001. Field assessment of nanoscale bimetallic particles for groundwater treatment. Environ. Sci. Technol. 35. 4922−4926.

Farrell, J., M. Kason, N. Melitas, T. Li. 2000. Investigation of the long-term performance of zero-valent iron for reductive dechlorination of trichloroethylene. Environ. Sci. Technol. 34. 514−521.

Flury, M., and H. Qiu. 2008. Modeling colloid-facilitated contaminant transport in the vadose zone. Vadose Zone J. 7. 682 – 697.

He, F. and D.Y. Zhao. 2005. Preparation and characterization of a new class of starch-stabilized bimetallic nanoparticles for degradation of chlorinated hydrocarbons in water. Environ. Sci. Technol. 39. 3314–3320.

He, F., D.Y. Zhao, J.C. Liu and C.B. Roberts. 2007. Stabilization of Fe–Pd nanoparticles with sodium carboxymethyl cellulose for enhanced transport and dechlorination of trichloroethylene in soil and groundwater, Ind. Eng. Chem. Res. 46. 29–34.

Hering, J and J.L. Schnoor. 2000. Chemical Speciation and Reactivity in Water Chemistry and Water Technology: A Symposium in Honor of James J. Morgan. Preprints of Extended Abstracts. 40 (2). 639-640.

Johnson, T. L., M. M Scherer, and P.G. Tratnyek. 1996. Kinetics of Halogenated Organic Compound Degradation by Iron Metal. Environ. Sci. Technol. 30. 2634.

Kanel, S. R. and H. Choi. 2007. Transport characteristics of surface-modified nanoscale zero-valent iron in porous media Water Sci. Technol. 55 (157). 162.

Klausen, J., P.J. Vikesland, T. Kohn, D.R. Burris, W.P. Ball, and A.L. Roberts. 2003. Longevity of granular iron in groundwater treatment processes: solution composition effects on reduction of organohalides and nitroaromatic compounds. Environ. Sci. Technol. 37. 1208−1218.

Lecoanet H., J. Bottero, and M. Wiesner. 2004. Laboratory assessment of the mobility of nanomaterials in porous media. Environ Sci Technol. 38. 5164–5169.

Lien, H.L., and W.X. Zhang. 1999. Transformation of chlorinated methanes by nanoscale iron particles. J. Environ. Eng. 125. 1042–1047.

Lin C.J., S.L. Lo, Y. H. Liou. 2004. Dechlorination of trichloroethylene in aqueous solution by noble metal-modified iron. Journal of Hazardous Materials. 116(3).219-228.

Liu, Y., S.A Majetich, R.D Tilton, D.S Sholl, G.V. Lowry. 2005. TCE Dechlorination Rates, Pathways, and Efficiency of Nanoscale Iron Particles with Different Properties. Environ. Sci. Technol. 39. 1338.

Liu, Y. and G.V Lowry, G. V. 2006. Effect of particle age (Fe0 content) and solution pH on NZVI reactivity: H_2 evolution and TCE dechlorination. Environ. Sci. Technol. 40. 6085.

Liu, Y., and T. Phenrat, G.V. Lowry. 2007. Effect of TCE concentration and dissolved groundwater solutes on NZVI-promoted TCE dechlorination and H_2 evolution Environ. Sci. Technol. 41. 7881.788.

Long, T and C. A. Ramsburg. 2010. Encapsulation of nZVI particles using a Gum Arabic stabilized oil-in-water emulsion. Journal of Hazardous Materials. Article in Press, Corrected Proof.

Meyer, D.E, S. Hampson, L. Ormsbee, and D. Bhattacharyya. 2009. A Study of Groundwater Matrix Effects for the Destruction of Trichloroethylene Using Fe/Pd Nanoaggregates. Environ Prog Sustain Energy. 28(4). 507–518.

Moore, A.M. and T.M. Young. 2005. Chloride interactions with iron surfaces: implications for perchlorate and nitrate remediation using permeable reactive barriers, J. Environ. Eng. 131. 924–933.

Pennell, K. D., G.A. Pope, and L.M. Abriola. 1996. Influence of Viscous and Buoyancy Forces on the Mobilization of Residual Tetrachloroethylene during Surfactant Flushing. Environ. Sci. Technol. 30 (4), 1328−1335.

Phenrat T., N. Saleh, K. Sirk, R.D. Tilton, and G.V Lowry. 2007. Aggregation and sedimentation of aqueous nanoscale zerovalent iron dispersions. Environ Sci Technol. 41. 284–290.

Phenrat T., D. Schoenfelder, M. Losi, J. Yi, S.A. Peck, and G.V. Lowry. 2007. Treatability Study for a TCE Contaminated Area using Nanoscale- and Microscale-Zerovalent Iron Particles: Reactivity and Reactive Life Time. Chapter 10. ACS Symposium Series (10).

Phenrat, T., H.J. Kim, F. Fagerlund, T. Illangasekare, R.D. Tilton, and G.V. Lowry. 2009. Particle size distribution, concentration, and magnetic attraction affects transport of polymer-modified Fe0 nanoparticles in sand columns. Environ. Sci. Technol. 43(13). 5079– 5085.

Phenrat, T., Y. Liu, R. Tilton, and G.V. Lowry. 2009. Adsorbed Polyelectrolyte Coatings Decrease Fe0 Nanoparticle Reactivity with TCE in Water: Conceptual Model and Mechanisms. Environmental Science & Technology. 43(5): 1507-1514.

Quinn J., C. Geiger, C. Clausen, K. Brooks, C. Coon, S. O'Hara, T. Krug, D. Major, W-S Yoon, Gavaskar A, and T. Holdsworth. 2005. Field demonstration of DNAPL dehalogenation using emulsified zero-valent iron. Environ Sci Technol 39(5). 1309–131.

Rao, P.S.C., M.D. Annable, R.K. Sillan, D. Dai, K. Hatfield, A.L. Wood, and W.D Graham. 1997. Field-scale evaluation of in situ cosolvent flushing for enhanced aquifer remediation. Water Resour. Res. 33. 2673–2686.

Sale, T.C. and D.B. McWhorter. 2001. Steady-state mass transfer from single-component dense non-aqueous phase liquids in uniform flow fields, Water Resour. 37. 393–404.

Saleh N., K. Sirk, Y. Liu, T. Phenrat, B. Dufour, K. Matyjaszewski, R.D. Tilton, G.V. Lowry. 2007. Surface modifications enhance nanoiron transport and NAPL targeting in saturated porous media. Environ Eng Sci. 24(1). 45–5.

Schrick B., J. Blough, A. Jones and T.E. Mallouk. 2002. Hydrodechlorination of trichloroethylene to hydrocarbons using bimetallic nickel-iron nanoparticles. Chem. Mater. 14(12), 5140–5147.

Schrick, B., B.W Hydutsky, J.L. Blough, T.E. Mallouk. 2004. Delivery vehicles for zerovalent metal nanoparticles in soil and groundwater. Chem. Mater. 16. 2187−2193.

Sivasanker,S. 2002. Catalyst Deactivation. Catalysis. Narosa Publishing House. 254-256.

Song, H. and E.R. Carraway. 2008. Catalytic hydrodechlorination of chlorinated ethenes by nanoscale zero-valent iron Appl. Catal. B. 78(1−2). 53. 6.

Soo, H. and C.J. Radke. 1984. Velocity Effects in Emulsion Flow Through Porous Media. J. Colloid Interface Sci. 102 (2). 462.

Suchomel, E.J. and K.D. Pennell. 2006. Reductions in contaminant mass discharge following partial mass removal from dnapl source zones, Environ. Sci. Technol. 40. 6110–6116.

Taghavy A., J. Costanza, K.D. Pennell, and L.M. Abriola. 2010. Effectiveness of nanoscale zero-valent iron for treatment of a PCE–DNAPL source zone. Journal of Contaminant Hydrology. 118(3-4).128-142.

Tee,Y.H, L. Bachas and D. Bhattacharyya. 2009. Degradation of trichloroethylene and dichlorobiphenyls by iron-based bimetallic nanoparticles. J. Phys. Chem. C. 113. 9454.

Tratnyek, P.G. and R.L. Johnson. 2006. Nanotechnologies for environmental cleanup. Nano Today. 1. 44–48.

UNC Chapel Hill CEP Capstone Class. 2005. Groundwater Exposure. Envionmental Risk.

Wang, C.-B., W. Zhang. 1997. Synthesizing Nanoscale Iron Particles for Rapid and Complete Dechlorination of TCE and PCBs. Environ. Sci. Technol. 31. 2154.

Wang W., M. Zhou, Z. Jin, and T. Li. 2010. Reactivity characteristics of poly(methyl methacrylate) coated nanoscale iron particles for trichloroethylene remediation. J Hazard Mater. 173(1-3). 724-30.

Wood, A.L., C.G. Enfield, F.P. Espinoza, M. Annable, M.C. Brooks, P.S.C. Rao, D. Sabatini, and R. Knox. 2005. Design of aquifer remediation systems: (2)

Estimating site-specific performance and benefits of partial source removal. J. Contam. Hydrol. 81. 148–166

Zhan, J., T. Zheng, G. Piringer, C. Day, G. McPherson, Y., and Lu, K. Papadopoulus and V. John. 2008. Transport characteristics of nanoscale functional zerovalent iron/silica composites for in situ remediation of trichloroethylene, Environmental Science & Technology. 42 (23). 8871–8876.

Zhang W., C. Wang and H. Lien. 1998. Catalytic reduction of chlorinated hydrocarbons by bimetallic particles. Catal. Today. 40(4),387–395.

Zhang W. 2003. Nanoscale iron particles for environmental remediation. J. Nanopart. Res. 5. 323−332.